Appendix A
Probability Distributions and Combination of Random Variables

A.1 Probability Density Functions

Normal (Gaussian) Distribution

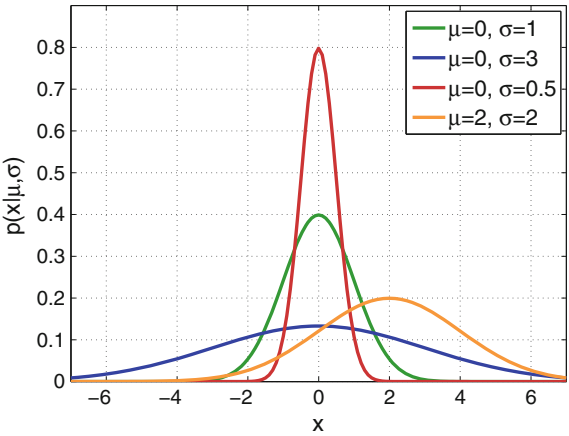

Fig. A.1 Probability density function of normal (Gaussian) random variables for different values of the parameters μ and σ

The stating point of most of the probability distributions that arises when dealing with noise in medical imaging is the Normal distribution, also known as Gaussian distribution. Let X be a random variable (RV) that follows a normal distribution. This is usually represented as follows:

$$X \sim N(\mu, \sigma^2)$$

where μ is the mean of the distribution and σ is the standard deviation.

S. Aja-Fernández and G. Vegas-Sánchez-Ferrero,
Statistical Analysis of Noise in MRI, DOI 10.1007/978-3-319-39934-8

PDF: (Probability density function)

$$p(x|\mu,\sigma) = \frac{1}{\sigma\sqrt{2\pi}} \exp\left(-\frac{(x-\mu)^2}{2\sigma^2}\right) \tag{A.1}$$

MGF: (Moment generating function)

$$M_X(t) = \exp\left(\mu t + \frac{\sigma^2 t^2}{2}\right)$$

Main parameters:

$$\begin{aligned} \text{Mean} &= \mu \\ \text{Median} &= \mu \\ \text{Mode} &= \mu \\ \text{Variance} &= \sigma^2 \end{aligned}$$

Main moments:

$$\begin{aligned} \mu_1 &= E\{x\} = \mu \\ \mu_2 &= E\{x^2\} = \mu^2 + \sigma^2 \\ \mu_3 &= E\{x^3\} = \mu^3 + 3\mu\sigma^2 \\ \mu_4 &= E\{x^4\} = \mu^4 + 6\mu^2\sigma^2 + 3\sigma^4 \end{aligned}$$

Rayleigh Distribution

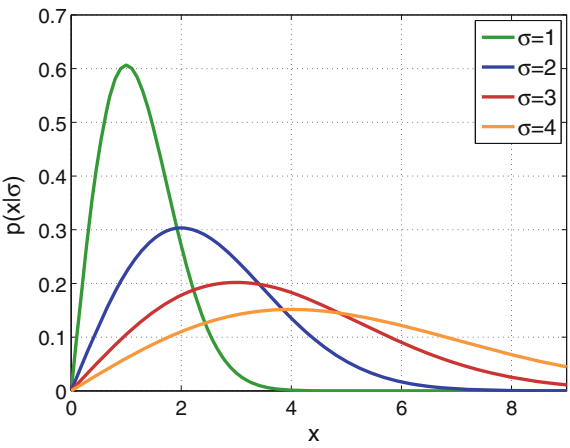

Fig. A.2 Probability density function of Rayleigh random variables for different values of the parameter σ

The Rayleigh distribution can be seen as the distribution that models the square root of the sum of squares of two independent and identically distributed Gaussian RV with the same σ and $\mu = 0$. This is the case, for instance of the modulus of a complex Gaussian RV with independent components:

$$R(\sigma) = \sqrt{X_1^2 + X_2^2}, \qquad X_i \sim N(0, \sigma^2)$$

$$R(\sigma) = \sqrt{(X_1 - \mu_1)^2 + (X_2 - \mu_2)^2}, \quad X_i \sim N(\mu_i, \sigma^2)$$

$$R(\sigma) = |X|, \qquad X = N(0, \sigma^2) + jN(0, \sigma^2)$$

PDF:

$$p(x|\sigma) = \frac{x}{\sigma^2} \exp\left(-\frac{x^2}{2\sigma^2}\right) \tag{A.2}$$

MGF:

$$M_X(t) = 1 + \sigma\, t\, e^{\sigma^2 t^2/2} \sqrt{\frac{\pi}{2}} \left(\text{erf}\left(\frac{\sigma t}{\sqrt{2}}\right) + 1\right)$$

Raw moments:

$$\mu_k = \sigma^k\, 2^{k/2}\, \Gamma(1 + k/2)$$

Main parameters:

$$\begin{aligned} \text{Mean} &= \sigma\sqrt{\frac{\pi}{2}} \\ \text{Median} &= \sigma\sqrt{\log 4} \\ \text{Mode} &= \sigma \\ \text{Variance} &= \frac{4 - \pi}{2}\sigma^2 \end{aligned}$$

Main moments:

$$\begin{aligned} \mu_1 &= \sqrt{\frac{\pi}{2}}\sigma \\ \mu_2 &= 2\,\sigma^2 \\ \mu_3 &= 3\,\sqrt{\frac{\pi}{2}}\sigma^3 \\ \mu_4 &= 8\,\sigma^4 \end{aligned}$$

Rician Distribution

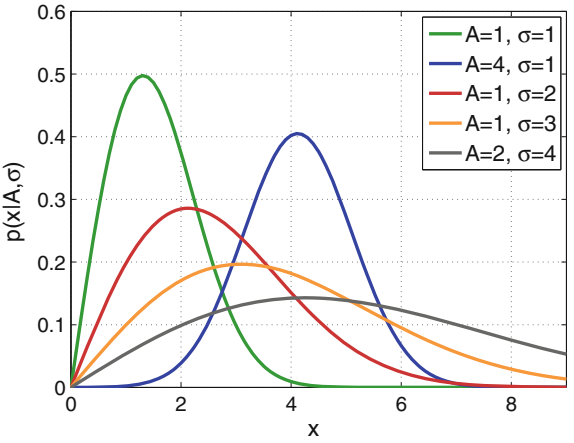

Fig. A.3 Probability density function of Rician random variables for different values of the parameters A and σ

The Rician distribution can be seen as the distribution that models the square root of the sum of squares of two independent and identically distributed Gaussian RV with the same σ.

$$R(A,\sigma) = \sqrt{X_1^2 + X_2^2}, \quad X_i \sim N(\mu_i, \sigma^2)$$

$$R(A,\sigma) = |X|, \quad X = N(\mu_1, \sigma^2) + jN(\mu_2, \sigma^2)$$

PDF:

$$p(x|A,\sigma) = \frac{x}{\sigma^2}\, e^{-\frac{x^2+A^2}{2\sigma^2}}\, I_0\left(\frac{Ax}{\sigma^2}\right) u(x), \tag{A.3}$$

where

$$A = \sqrt{\mu_1^2 + \mu_2^2}.$$

For $A = 0$ the Rician distribution simplifies to a Rayleigh.

Raw moments

$$\mu_k = \sigma^k\, 2^{k/2}\, \Gamma(1 + k/2)\, L_{k/2}\left(-\frac{A^2}{2\sigma^2}\right)$$

where $L_n(x)$ is the Laguerre polynomial. It is related to the confluent hypergeometric function of the first kind:

$$L_n(x) = {}_1F_1(-n; 1; x).$$

The even moments become simple polynomials.

Main moments:

$$\mu_1 = \sqrt{\frac{\pi}{2}} L_{1/2}\left(-\frac{A^2}{2\sigma^2}\right)\sigma$$
$$\mu_2 = A^2 + 2\,\sigma^2$$
$$\mu_3 = 3\sqrt{\frac{\pi}{2}}\, L_{3/2}\left(-\frac{A^2}{2\sigma^2}\right)\sigma^3$$
$$\mu_4 = A^4 + 8\,\sigma^2 A^2 + 8\,\sigma^4$$

$$\text{Var} = 2\sigma^2 + A^2 - \frac{\pi\sigma^2}{2} L_{1/2}^2\left(-\frac{A^2}{2\sigma^2}\right)$$
$$\approx \sigma^2\left(1 - \frac{1}{4x} - \frac{1}{8x^2} + O(x^{-3})\right) \quad \text{with } x = \frac{A^2}{2\sigma^2}$$

Series Expansion of Hypergeometric Functions

$$L_{1/2}(-x) = \frac{2\sqrt{x}}{\sqrt{\pi}} + \frac{1}{2\sqrt{\pi}\sqrt{x}} + \frac{1}{16\sqrt{\pi}x^{3/2}} + O\left(x^{-5/2}\right)$$

$$L_{3/2}(-x) = \frac{4x^{3/2}}{3\sqrt{\pi}} + \frac{3\sqrt{x}}{\sqrt{\pi}} + \frac{3}{8\sqrt{\pi}\sqrt{x}} + \frac{1}{32\sqrt{\pi}x^{3/2}} + O\left(x^{-5/2}\right).$$

Central Chi Distribution (c-χ)

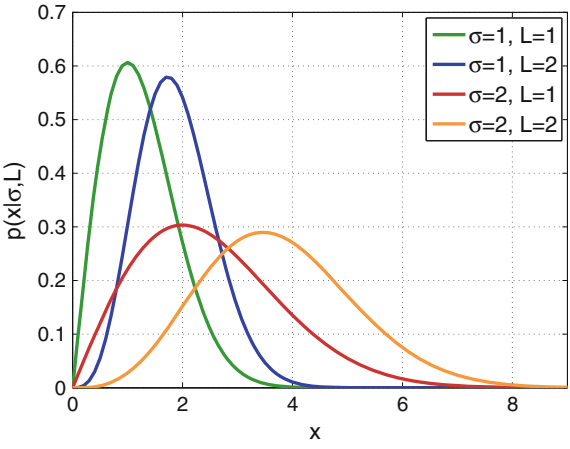

Fig. A.4 Probability density function of c-χ random variables for different values of the parameters L and σ

The central-χ (c-χ) distribution can be seen as the distribution that models the square root of the sum of squares of several independent and identically distributed Gaussian RV with the same σ and $\mu = 0$:

$$R(L,\sigma) = \sqrt{\sum_{i=1}^{2L} X_i^2 X_i} \sim N(0,\sigma^2)$$

$$R(L,\sigma) = \sqrt{\sum_{i=1}^{2L} (X_i - \mu_i)^2 X_i} \sim N(\mu_i,\sigma^2)$$

$$R(L,\sigma) = \sqrt{\sum_{i=1}^{L} |Y_i|^2} \quad Y_i = N(0,\sigma^2) + jN(0,\sigma^2).$$

PDF:

$$p(x|\sigma,L) = \frac{2^{1-L}}{\Gamma(L)} \frac{x^{2L-1}}{\sigma^{2L}} e^{-\frac{x^2}{2\sigma^2}} \tag{A.4}$$

Note that this definition of the (nonnormalized) PDF uses parameters related to MRI configuration. In other texts, $m = 2L$ are used instead. The Rayleigh distribution is a special case of the c-χ when $L = 1$.

Raw moments:

$$\mu_k = \sigma^k 2^{k/2} \frac{\Gamma(k/2+L)}{\Gamma(L)}.$$

For n an integer,

$$\Gamma(n) = (n-1)!$$

and

$$\Gamma\left(n+\frac{1}{2}\right) = \frac{\sqrt{\pi}}{2^n} \prod_{k=1}^{n} (2k-1)$$

Main moments:

$$\mu_1 = \sqrt{2}\, \frac{\Gamma(L+1/2)}{\Gamma(L)}\, \sigma$$
$$\mu_2 = 2\, L\, \sigma^2$$

$$\mu_3 = 3\sqrt{2}\,\frac{\Gamma(L+3/2)}{\Gamma(L)}\,\sigma^3$$
$$\mu_4 = 4\,L(L+1)\,\sigma^4$$

$$\text{Var} = 2\sigma^2\left(L - \left(\frac{\Gamma(k/2+L)}{\Gamma(L)}\right)^2\right)$$

Noncentral Chi Distribution (nc-χ)

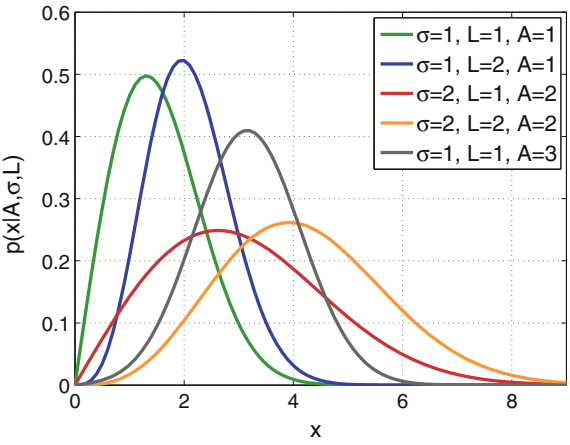

Fig. A.5 Probability density function of nc-χ random variables for different values of the parameters A, L and σ

The noncentral-χ (nc-χ) distribution can be seen as the distribution that model the square root of the sum of squares of several independent and identically distributed Gaussian RV with the same σ:

$$R = \sqrt{\sum_{i=1}^{2L} X_i^2} \quad X_i \sim N(\mu_i, \sigma^2)$$

$$R = \sqrt{\sum_{i=1}^{L} |Y_i|^2} \quad Y_i = N(\mu_{1,i}, \sigma^2) + jN(\mu_{2,i}, \sigma^2)$$

PDF:

$$p(x|A_L, \sigma, L) = \frac{A_L^{1-L}}{\sigma^2} x^L e^{-\frac{x^2+A_L^2}{2\sigma^2}} I_{L-1}\left(\frac{A_L x}{\sigma^2}\right) u(x), \tag{A.5}$$

with

$$A_L = \sqrt{\sum_{i=1}^{L} |\mu_i|^2}.$$

When $A_L = 0$ the nc-χ simplifies into a c-χ. The Rician distribution is a special case of the nc-χ for $L = 1$.

Main moments:

$$\mu_1 = \sqrt{2}\,\frac{\Gamma(L+1/2)}{\Gamma(L)}\,{}_1F_1\left(-\frac{1}{2}, L, -\frac{A_L^2}{2\sigma^2}\right)\sigma$$
$$\mu_2 = A_L^2 + 2\,L\sigma^2$$
$$\mu_3 = 3\sqrt{2}\,\frac{\Gamma(L+3/2)}{\Gamma(L)}\,{}_1F_1\left(-\frac{3}{2}, L, -\frac{A_L^2}{2\sigma^2}\right)\sigma^3$$
$$\mu_4 = A_L^4 + 4(L+1)A_L^2\,\sigma^2 + 4L(L+1)\,\sigma^4$$

$$\text{Var} = 2\sigma^2\left(1 + x - \left(\frac{\Gamma(L+1/2)}{\Gamma(L)}\right)^2 {}_1F_1{}^2\left(-\frac{1}{2}, L, -x\right)\right)$$
$$\approx \sigma^2\left(1 + \frac{1-2L}{4x} + \frac{3-8L+4L^2}{8x^2} + O(x^{-3})\right) \quad \text{with } x = \frac{A^2}{2\sigma^2}$$

Central Chi Square Distribution (c-χ^2)

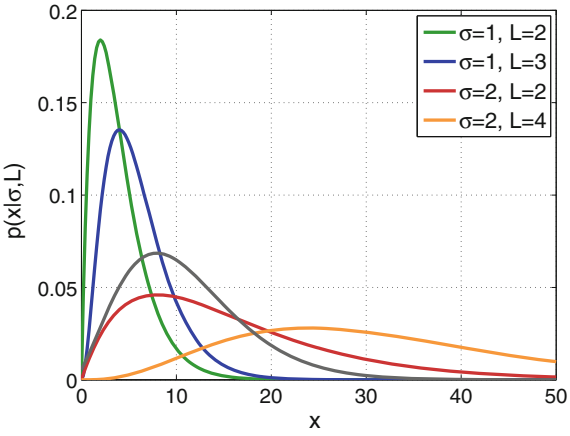

Fig. A.6 Probability density function of c-χ^2 random variables for different values of the parameters L and σ

The central-χ square (c-χ^2) distribution can be seen as the distribution that models the square root of the sum of several independent and identically distributed Gaussian RV with the same σ and $\mu = 0$:

$$R(L,\sigma) = \sum_{i=1}^{2L} X_i^2 X_i \sim N(0,\sigma^2)$$

$$R(L,\sigma) = \sum_{i=1}^{2L} (X_i - \mu_i)^2 X_i \sim N(\mu_i,\sigma^2)$$

$$R(L,\sigma) = \sum_{i=1}^{L} |Y_i|^2 \quad Y_i = N(0,\sigma^2) + jN(0,\sigma^2).$$

PDF:

$$p(x|\sigma,L) = \frac{1}{2\sigma^2\Gamma(L)}\left(\frac{x}{2\sigma^2}\right)^{L-1} e^{-\frac{x}{2\sigma^2}} u(x), \tag{A.6}$$

Raw moments:

$$\mu_k = \sigma^{2k} 2^k \frac{\Gamma(k+L)}{\Gamma(L)}.$$

Main moments:

$$\mu_1 = 2\,L\,\sigma^2$$
$$\mu_2 = 4\,L(L+1)\,\sigma^4$$

Noncentral Chi Square Distribution (nc-χ^2)

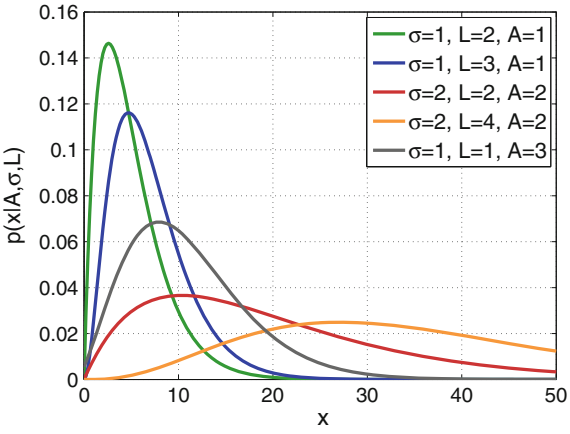

Fig. A.7 Probability density function of nc-χ^2 random variables for different values of the parameters A, L and σ

The noncentral-χ square (nc-χ^2) distribution can be seen as the distribution that model the square root of the sum of several independent and identically distributed Gaussian RV with the same σ:

$$R = \sum_{i=1}^{2L} X_i^2 \quad X_i \sim N(\mu_i, \sigma^2)$$

$$R = \sum_{i=1}^{L} |Y_i|^2 \quad Y_i = N(\mu_{1,i}, \sigma^2) + jN(\mu_{2,i}, \sigma^2)$$

PDF:

$$p(x|A_L, \sigma, L) = \frac{A_L^{1-L}}{2\sigma^2} x^{\frac{1}{2}(L-1)} e^{-\frac{x+A_L^2}{2\sigma^2}} I_{L-1}\left(\frac{A_L\sqrt{x}}{\sigma^2}\right) u(x), \tag{A.7}$$

with

$$A_L^2 = \sum_{i=1}^{L} |\mu_i|^2.$$

Main moments:

$$\mu_1 = A_L^2 + 2\,L\sigma^2$$
$$\mu_2 = A_L^4 + 4(L+1)A_L^2\,\sigma^2 + 4L(L+1)\,\sigma^4$$

Gamma Distribution

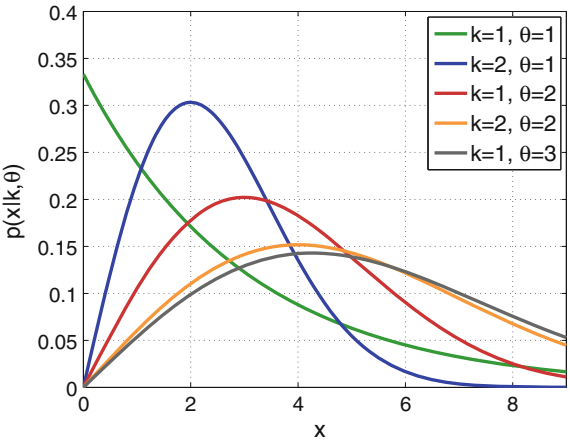

Fig. A.8 Probability density function of Gamma random variables for different values of the parameters k, θ

The Gamma distribution is a continuous probability distribution that can be used in many different situations in medical imaging to model the data. It models the variance of Gaussian data [14], and in MRI it has been used to approximate the local variance of Rician, Rayleigh, c-χ and nc-χ [15].

PDF:

$$p(x|k,\theta) = x^{k-1}\frac{\exp(-x/\theta)}{\Gamma(k)\theta^k}u(x) \tag{A.8}$$

Note that this distribution equals a c-χ^2 when $k = L$ and $\theta = 2\sigma^2$.

MGF:

$$M_X(t) = (1-\theta t)^{-k} \text{ for } t < 1/\theta$$

Main parameters:

$$\begin{aligned}\text{Mean} &= k\theta\\ \text{Median} &= —\\ \text{Mode} &= (k-1)\theta\\ \text{Variance} &= k\theta^2\end{aligned}$$

Folded Normal Distribution

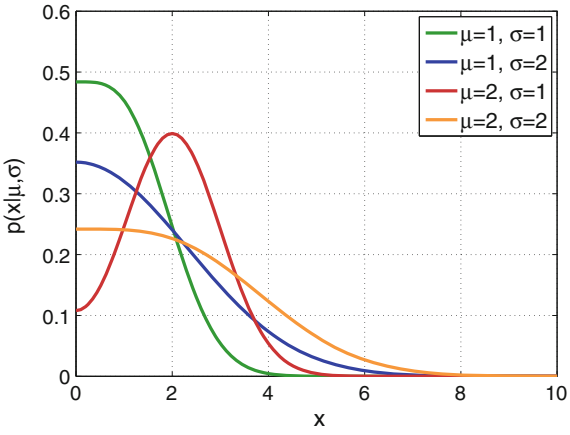

Fig. A.9 Probability density function of folded normal random variables for different values of the parameters μ, and σ

The folded normal distribution is the probability distribution of the absolute value of a Gaussian random variable

$$F_N(\mu,\sigma^2) = |X|, \quad X \sim N(\mu,\sigma^2);$$

PDF:

$$p(x|\mu,\sigma^2) = \left(\frac{1}{\sqrt{2\pi\sigma^2}}\, e^{-\frac{(x-\mu)^2}{2\sigma^2}} + \frac{1}{\sqrt{2\pi\sigma^2}}\, e^{-\frac{(x+\mu)^2}{2\sigma^2}}\right) u(x) \tag{A.9}$$

or alternatively

$$p(x|\mu,\sigma^2) = \sqrt{\frac{2}{\pi\sigma^2}} e^{-\frac{(x^2+\mu^2)}{2\sigma^2}} \cosh\left(\frac{\mu x}{\sigma^2}\right) u(x). \tag{A.10}$$

Main moments:

$$\mu_1 = \sigma\sqrt{\frac{2}{\pi}}\, \exp\left(\frac{-\mu^2}{2\sigma^2}\right) - \mu\, \mathrm{erf}\left(\frac{-\mu}{\sqrt{2\sigma^2}}\right)$$
$$\mu_2 = \mu^2 + \sigma^2$$
$$\mathrm{Var} = \mu^2 + \sigma^2 - \mu_1^2$$

Half-Normal Distribution

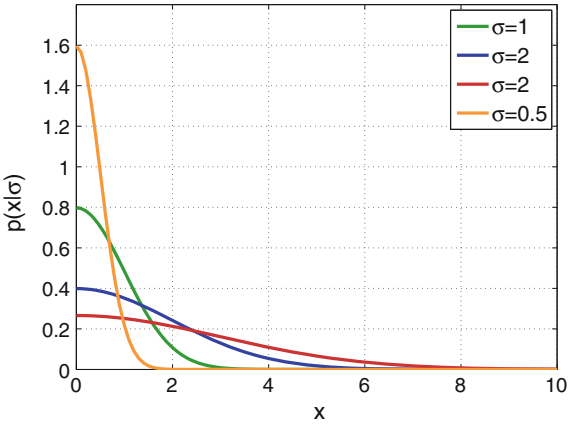

Fig. A.10 Probability density function of Half Normal random variables for different values of the parameter σ

The half-normal distribution is a special case of the folded normal distribution with $\mu = 0$:

$$H_N(\sigma^2) = |X|, \quad X \sim N(0,\sigma^2);$$

PDF:

$$p(x|\sigma^2) = \frac{\sqrt{2}}{\sigma\sqrt{\pi}} \exp\left(-\frac{x^2}{2\sigma^2}\right) u(x) \tag{A.11}$$

Main moments:

$$\mu_1 = \sqrt{2/\pi}\sigma$$
$$\mu_2 = \sigma^2$$
$$\text{Var} = \sigma^2\left(1 - \frac{2}{\pi}\right)$$

A.2 Combination of Random Variables

A.2.1 Combination of Gaussian Random Variables

To define the probability distributions of the noise in the different MRI modalities, we will make use of the following combinations of Gaussian random variables:

1. Let X be a complex Gaussian RV, $X = X_r + j \cdot X_i$, $X_r \sim N(\mu_1, \sigma^2)$, $X_i \sim N(\mu_2, \sigma^2)$, with the real and imaginary parts being independent and identically distributed (IID). The modulus of X:

$$R(A, \sigma^2) = |X| = \sqrt{X_r^2 + X_i^2}$$

follows a **Rician distribution** with parameters $A = |\mu_1^2 + \mu_2^2|$ and σ^2:

$$|N(\mu_1, \sigma^2) + j \cdot N(\mu_2, \sigma^2)| \sim \text{Rician}\ (A, \sigma^2). \tag{A.12}$$

2. Let X be a complex Gaussian RV with zero mean, $X = X_r + j \cdot X_i$, $X_r \sim N(0, \sigma^2)$, $X_i \sim N(0, \sigma^2)$ with the real and imaginary parts being IID. The modulus of X:

$$R(\sigma^2) = |X| = \sqrt{X_r^2 + X_i^2}$$

follows a **Rayleigh** distribution with parameter σ^2:

$$|N(0, \sigma^2) + j \cdot N(0, \sigma^2)| \sim \text{Rayleigh}\ (\sigma^2). \tag{A.13}$$

3. **Linear combination of Gaussian RV:** Let $X \sim N(\mu, \sigma^2)$ be a Gaussian RV. The linear combination:

$$\alpha + \beta \cdot X$$

follows a Gaussian distribution with parameters $\alpha + \mu$ and $\beta^2\sigma^2$:

$$\alpha + \beta \cdot X \sim N(\alpha + \mu, \beta^2\sigma^2). \tag{A.14}$$

4. **Summation of Gaussian RVs:** Let X_i be a set of L IID complex Gaussian RV, $X_i \sim N(\mu_i, \sigma_i^2)$. Then, the sum

$$\sum_{i=1}^{L} X_i$$

follows a Gaussian distribution with parameters $\mu_T = \sum_{i=1}^{L} \mu_i$ and $\sigma_T^2 = \sum_{i=1}^{L} \sigma_i^2$:

$$\sum_{i=1}^{L} X_i \sim N\left(\mu_T, \sigma_T^2\right). \tag{A.15}$$

5. **Weighted sum of Gaussian RVs:** Let X_i be a set of L correlated complex Gaussian RV, i.e., a multivariate Gaussian RV with zero mean and covariance matrix $\mathbf{\Sigma}$. Then, the combination

$$\sum_{i=1}^{L} \omega_i X_i$$

follows a Gaussian distribution with zero mean and covariance $\mathbf{\Sigma}^* = \mathbf{W}^H \mathbf{\Sigma}\, \mathbf{W}$, with $\mathbf{W} = [\omega_1, \ldots, \omega_L]^T$:

$$\sum_{i=1}^{L} \omega_i X_i \sim N\left(0, \mathbf{W}^H \mathbf{\Sigma}\, \mathbf{W}\right). \tag{A.16}$$

6. Let $X_l = X_{r_l} + j \cdot X_{i_l}$, $X_{r_l} \sim N(\mu_l, \sigma^2)$, $X_{i_l} \sim N(\mu_l, \sigma^2)$ be a set of L IID complex Gaussian RV with means μ_i and identical variance σ^2. Then, the combination

$$\sqrt{\sum_{l=1}^{L} |X_l|^2} = \sqrt{\sum_{l=1}^{L} (X_{r_l}^2 + X_{i_l}^2)}$$

follows a noncentral-χ (nc-χ) distribution with $2L$ degrees of freedom and parameters $\sum_{l=1}^{L} \mu_l$ and σ^2.

7. Let $X_l = X_{r_l} + j \cdot X_{i_l}$, $X_{r_l} \sim N(0, \sigma^2)$, $X_{i_l} \sim N(0, \sigma^2)$ be a set of L IID complex Gaussian RV with zero mean and identical variance σ^2. Then, the combination

$$\sqrt{\sum_{l=1}^{L} |X_l|^2} = \sqrt{\sum_{l=1}^{L} (X_{r_l}^2 + X_{i_l}^2)}$$

follows a central-χ (c-χ) distribution with $2L$ degrees of freedom and parameter σ^2.

8. Let $X_l = X_{r_l} + j \cdot X_{i_l}$, $X_{r_l} \sim N(\mu_l, \sigma^2)$, $X_{i_l} \sim N(\mu_l, \sigma^2)$ be a set of L IID complex Gaussian RV with means μ_i and identical variance σ^2. Then, the combination

$$\sum_{l=1}^{L} |X_l|^2 = \sqrt{\sum_{l=1}^{L} (X_{r_l}^2 + X_{i_l}^2)}$$

follows a noncentral-χ square (nc-χ^2) distribution with $2L$ degrees of freedom and parameters $\sum_{l=1}^{L} \mu_l$ and σ^2.

9. Let $X_l = X_{r_l} + j \cdot X_{i_l}$, $X_{r_l} \sim N(0, \sigma^2)$, $X_{i_l} \sim N(0, \sigma^2)$ be a set of L IID complex Gaussian RV with zero mean and identical variance σ^2. Then, the combination

$$\sum_{l=1}^{L} |X_l|^2 = \sqrt{\sum_{l=1}^{L} (X_{r_l}^2 + X_{i_l}^2)}$$

follows a central-χ square (c-χ^2) distribution with $2L$ degrees of freedom and parameter σ^2:

$$\sum_{l=1}^{L} |N_l(0, \sigma^2)|^2 \sim \text{c-}\chi^2 \left(2L, \sigma^2\right). \tag{A.17}$$

10. Note that if $X_l = X_{r_l} + j \cdot X_{i_l}$ is a set of L correlated complex Gaussian RVs, i.e., a multivariate Gaussian RV with covariance matrix $\mathbf{\Sigma}$, the combination

$$X = \sqrt{\sum_{l=1}^{L} |N_l(\mu_l, \sigma_l^2)|^2}$$

will not follow a nc-χ distribution. The same happens for a set of IID Gaussian variables $X_l \sim N(\mu_l, \sigma^2)$ with the same variance, whenever the combination is done using different weights ω_l:

$$\sqrt{\sum_{l=1}^{L} |\omega_l \cdot X_l|^2}.$$

11. **Product of Gaussian variables:** Let $X_1 \sim N(0, \sigma_1^2)$ and $X_2 \sim N(0, \sigma_2^2)$ be a couple of IID complex Gaussian RV. Then, the sum product

$$S = X_1 \times X_2$$

follows a normal product distribution with PDF:

$$p(x|\sigma_1, \sigma_2) = \frac{1}{\pi\sigma_1\sigma_2} K_0\left(\frac{|x|}{\sigma_1\sigma_2}\right).$$

12. **Sum of squares of Gaussian variables:** Let $X_i \sim N(0, \sigma^2)$ be a set of L IID Gaussian random variables with zero mean the same variance σ. The summation can be modeled by a Gamma distribution with parameters $k = \frac{L}{2}$ and $\theta = 2\sigma^2$:

$$S = \sum_{i=1}^{L} X_i^2(\sigma^2) \sim \gamma(L/2, 2\sigma^2).$$

13. **Sample variance of Gaussian variables:** Let $X_i \sim N(\mu_i, \sigma^2)$ be a set of L IID Gaussian random variables with the same variance σ. The sample variance is modeled by a Gamma distribution with parameters $k = \frac{L-1}{2}$ and $\theta = \frac{2\sigma^2}{L-1}$

$$S^2 = \frac{1}{L-1}\sum_{i=1}^{L}(X_i - \bar{X})^2 \sim \gamma\left(\frac{L-1}{2}, \frac{2\sigma^2}{L-1}\right).$$

A.2.2 Combination of Rayleigh Variables

Let $R_i(\sigma^2), i = 1, \ldots, N$ be a set of Rayleigh random variables.

1. **Sum of square Rayleigh variables:** the sum of squares of Rayleigh RVs is a Gamma distribution with parameters $k = N$ and $\theta = 2\sigma^2$:

$$S = \sum_{i=1}^{N} R_i^2(\sigma^2) \sim \gamma(N, 2\sigma^2).$$

2. **Sample mean of square Rayleigh variables:** the sample mean of squares of Rayleigh RVs is a Gamma distribution with parameters $k = N$ and $\theta = 2\sigma^2/N$:

$$S = \frac{1}{N}\sum_{i=1}^{N} R_i^2(\sigma^2) \sim \gamma\left(N, \frac{2\sigma^2}{N}\right).$$

3. **Sum of Rayleigh variables:** the PDF of the sum of Rayleigh variables

$$S = \sum_{i=1}^{N} R_i(\sigma^2)$$

can be approximated by [27]

$$p_x(x) = x^{2N-1} \frac{e^{-x^2/(2bN)}}{2^{N-1} N^N b^N \Gamma(N)} u(x)$$

with

$$b = \frac{\sigma^2}{N}[(2N-1)!!]^{1/N}] \approx \sigma^2 \frac{2}{e} \approx \sigma^2 \frac{\pi}{4}.$$

4. **Sample mean of Rayleigh variables:**

$$S = \frac{1}{N} \sum_{i=1}^{N} R_i(\sigma^2)$$

with approximated PDF [3, 27]:

$$p_x(x) = x^{2N-1} \frac{N^N}{2^{N-1} b^N \Gamma(N)} e^{-x^2 N/(2b)} u(x)$$

5. **Square sample mean of Rayleigh variables:**

$$S = \left(\frac{1}{N} \sum_{i=1}^{N} R_i(\sigma^2) \right)^2 \sim \gamma(N/2, 2b)$$

can be approximated by a Gamma distribution with parameters $k = N/2$ and $\theta = 2b$.

6. **Square root of sum of square Rayleigh variables:**

$$S = \sqrt{\sum_{i=1}^{L} R_i^2(\sigma^2)} \sim \text{c-}\chi(L, \sigma^2).$$

A.2.3 Combination of Rician Variables

Let $R_i(A_i, \sigma^2)$, $i = 1, \ldots, N$ be a set of Rician random variables.

1. **Sum of square Rician variables:**

$$S = \sum_{i=1}^{N} R_i^2(A_i, \sigma^2) \sim \text{nc-}\chi^2_{2N} \left(\frac{x}{\sigma^2}, \frac{A_N^2}{\sigma^2} \right)$$

with $\chi^2_{2N}()$ a nc-χ^2 with $2N$ degrees of freedom and $A_N^2 = \sum_i |A_i|^2$.

2. **Sample mean of square Rician variables:**

$$S = \frac{1}{N}\sum_{i=1}^{L} R_i^2(A_i, \sigma^2) \sim \chi^2_{2N}\left(\frac{xN}{\sigma^2}, \frac{A_N^2}{\sigma^2}\right).$$

3. **Sum of square Rician variables:** The summation of Rician RV

$$S = \sum_{i=1}^{L} R_i(A_i, \sigma^2)$$

can be approximated [105] by the PDF

$$p(t) = \frac{t^L}{c_2^2}\left(\frac{c_1}{c_2 b}\right)^{L-1} e^{-\frac{t^2}{2c_2^2} - \frac{b^2}{2c_1^2}} I_{L-1}\left(\frac{tb}{c_1 c_2}\right)$$

with c_1 and c_2 constants, $t = x/\sqrt{L}$ and $b = \sqrt{\frac{LK\Omega}{K+1}}$.

A.3 Sample Local Variance (Gamma Approximation)

In [15], authors proposed to approximate the distribution of the sample local variance of the different areas of a MRI image by Gamma distributions. This simplifications implies a reduction in the complexity of the actual distributions that allows to use that information for filtering, modeling and/or estimation procedures.

The (biased) sample local variance (SLV) of an image $M(\mathbf{x})$ is defined as

$$\mathcal{V}_{\mathbf{x}}(M(\mathbf{x})) = \frac{1}{|\eta(\mathbf{x})|}\sum_{\mathbf{p}\in\eta(\mathbf{x})} M^2(\mathbf{p}) - \left(\frac{1}{|\eta(\mathbf{x})|}\sum_{\mathbf{p}\in\eta(\mathbf{x})} M(\mathbf{p})\right)^2 \tag{A.18}$$

with $\eta(\mathbf{x})$ a neighborhood centered in $\mathbf{x}$. If $N = |\eta(\mathbf{x})|$, we define the random variable $V = \mathcal{V}_{\mathbf{x}}(M(\mathbf{x}))$ with moments

$$
\begin{aligned}
E\{V\} &= \left(1 - \frac{1}{N}\right)\left(\mu_2 - \mu_1^2\right) \\
E\{V^2\} &= \frac{1}{N^3}[(N^2 - 2N + 1)\mu_4 + (N^3 - 3N^2 + 5N - 3)\mu_2^2 \\
&\quad +(-2N^3 + 12N^2 - 22N + 12)\mu_2\mu_1^2 \\
&\quad +(N^3 - 6N^2 + 11N - 6)\mu_1^4 + (-4N^2 + 6N - 4)\mu_3\mu_1] \\
\mathrm{Var}(V) &= \frac{1}{N^3}\left[(-4N^2 + 8N - 4)\mu_3\mu_1 + (8N^2 - 20N + 12)\mu_2\mu_1^2\right. \\
&\quad +(-N^2 + 4N - 3)\mu_2^2 + +(N^2 - 2N + 1)\mu_4 \\
&\quad \left.+(-4N^2 + 10N - 6)\mu_1^4\right]
\end{aligned}
$$

For the main models used to model MRI data in this book:

Rayleigh

$$
\begin{aligned}
E\{V\} &= 2\sigma^2\left(1 - \frac{\pi}{4}\right)\left(\frac{N-1}{N}\right) \approx 2\sigma^2\left(1 - \frac{\pi}{4}\right) \\
\sigma_V^2 &= \frac{\sigma^4}{N}\left(4 + 2\pi - \pi^2 + O\left(\frac{1}{N}\right)\right) \approx \frac{\sigma^4}{N}(4 + 2\pi - \pi^2)
\end{aligned}
$$

Rician

$$
\begin{aligned}
E\{V\} &= \frac{(N-1)\sigma^2}{N}\left(1 - \frac{1}{4x} - \frac{1}{8x^2} + O\left(x^{-3}\right)\right) \approx \frac{(N-1)\sigma^2}{N} \\
\sigma_V^2 &= \frac{(N-1)\sigma^4}{N^2}\left(2 - \frac{1}{x} + \frac{3(2 - 5N + 3N^2)}{8N(N-1)x^2} + O\left(x^{-3}\right)\right) \approx \frac{2(N-1)\sigma^4}{N^2}
\end{aligned}
$$

with $x = \frac{A^2}{2\sigma^2}$.

Central Chi

$$
\begin{aligned}
E\{V\} &= \frac{2\sigma^2(N-1)}{N}\left(L - \left(\frac{\Gamma(L + 1/2)}{\Gamma(L)}\right)^2\right) \\
\sigma_V^2 &= \frac{4\sigma^4}{N}\left(L + 8L\frac{\Gamma^2(L + 1/2)}{\Gamma^2(L)}\right. \\
&\quad \left. -4\frac{\Gamma^4(L + 1/2)}{\Gamma^4(L)} - 4\frac{\Gamma(L + 1/2)\Gamma(L + 3/2)}{\Gamma^2(L)}\right) + O\left(\frac{1}{N^2}\right)
\end{aligned}
$$

with $K(L) = \left(L - \frac{\Gamma^2(L+1/2)}{\Gamma^2(L)}\right)$.

Noncentral Chi

$$E\{V\} = \frac{\sigma^2(N-1)}{N}\left(1 + \frac{1-2L}{x} + \frac{3-8L+4L^2}{8x^2} + O\left(x^{-3}\right)\right) \approx \frac{\sigma^2(N-1)}{N}$$
$$\sigma_V^2 = \frac{\sigma^4(N-1)}{N^2}\left(2 + \frac{1-2L}{x} + O\left(x^{-2}\right)\right) \approx \frac{2\sigma^4(N-1)}{N^2}$$

On the four cases, the PDF of the SLV may be approximated using a Gamma distribution. Parameters k and θ can be easily derived from mean and variance:

$$k = \frac{E^2\{V\}}{\sigma_V^2}, \qquad \theta = \frac{\sigma_V^2}{E^2\{V\}}$$

The mode of the distribution is one of the parameters used for noise estimation in this book. It can be calculated as

$$\text{mode}\{V\} = (k-1)\theta = E\{V\} - \frac{\sigma_V^2}{E\{V\}}$$

For each of the considered cases:

Rayleigh

$$\text{mode}\{V\} = \sigma^2\left(2 - \frac{\pi}{2} - \frac{1}{N}\left(\frac{5\pi^2 - 16\pi}{2\pi - 8}\right) + O(1/N^2)\right) \approx \sigma^2\left(2 - \frac{\pi}{2}\right)$$

Rician

$$\text{mode}\{V\} = \sigma^2\left(1 - \frac{3}{N} + O\left((\sigma/A)^2\right)\right) \approx \sigma^2$$

Central Chi

$$\text{mode}\{V\} = \sigma^2\left(L - \frac{\Gamma^2(L+1/2)}{\Gamma^2(L)}\right) + O\left(\frac{1}{N}\right) \approx 2K(L)\sigma^2$$

Noncentral Chi

$$\text{mode}\{V\} = \sigma^2\left(1 - \frac{3}{N} + O\left((\sigma/A)^2\right)\right) \approx \sigma^2$$

Appendix B
Variance-Stabilizing Transformation

The variance-stabilizing transformation (VST) has lately gained importance in the image processing field. In the case of MRI, this methodology has mainly focused on signal-dependent noise removal procedures [81, 146].

The fundamental goal of VST is to provide a set of transformations of random variables to render their distributions more tractable. Specifically, the VST tries to provide a function that transforms a random variable (RV) such that the variance of the transformed RV becomes constant, i.e., we are interested in a transformation $f_{\text{stab}}: \mathbb{R} \mapsto \mathbb{R}$ that leads to a random variable with a constant variance $\text{Var}\{f_{\text{stab}}(M)\} = 1$. This can be asymptotically approximated by considering the first-order expansion of $f_{\text{stab}}(M|\sigma)$ and imposing $\text{Var}\{f_{\text{stab}}(M|\sigma)\} = 1$.

The VST principle has recently gained a lot of attention in digital image processing field, both in theoretical and application aspects. In the field of medical imaging, the VST is principally used to deal with Poisson [147, 257], Poisson–Gaussian [34, 147], and Rician noise [81]. In the context of MRI, it is a particularly useful methodology, since it has been applied to efficiently solve different image processing problems such as stationary signal-dependent noise estimation [81], image denoising [146, 252, 258], and diffusion-weighted MR data reconstructions [204].

In the most fundamental way, the transformation applied to a certain random variable X can be derived using the first-order Taylor approximation of $f_{\text{stab}}(\cdot|\sigma)$ about μ:

$$f_{\text{stab}}(x|\sigma) = f_{\text{stab}}(\mu|\sigma) + (x - \mu) \left.\frac{df_{\text{stab}}}{dM}\right|_{x=\mu} + R_1(x, \mu), \tag{B.1}$$

where $R_1(x, \mu)$ is the remainder term of the expansion.

Now neglecting the term $R_1(x, \mu)$ and considering a RV X and μ its mean value, one can calculate the variance on both sides of Eq. (B.1):

$$\text{Var}\{f_{\text{stab}}(X|\sigma)\} \approx \text{Var}\{X|\mu, \sigma\} \cdot \left(\left.\frac{df_{\text{stab}}(z|\sigma)}{dz}\right|_{z=\mu} \right)^2. \tag{B.2}$$

S. Aja-Fernández and G. Vegas-Sánchez-Ferrero,
Statistical Analysis of Noise in MRI, DOI 10.1007/978-3-319-39934-8

Finally, imposing $\mathrm{Var}\{f_{\mathrm{stab}}(X|\sigma)\} = 1$, the function can be derived as the indefinite integral of Eq. (B.2) we have the general formula of VST for Rician RV [81]:

$$f_{\mathrm{stab}}(M|\sigma) = \int^{M} \frac{1}{\sqrt{\mathrm{Var}\{M|z,\sigma\}}} dz, \tag{B.3}$$

where $\mathrm{Var}\{M|z,\sigma\}$ is the conditional variance of M, i.e., the variance of the RV M expressed as a function of the central parameter z. The Eq. (B.3) defines the transformation f_{stab}, which turns the heteroscedastic RV into a homoscedastic RV.

B.1 VST for Rician Distributed Data

B.1.1 Asymptotic Stabilizer for Rician Distributed Data

The VST previously presented in now put into the context of Rician noise, in order to use it in MRI. Without loss of generality, we use the symbol $M\colon \Omega \to \mathbb{R}$ to denote both a real-valued Rician random variable (RV) and its realization (an observation). Let us assume now that M follows a stationary Rician distribution with noncentrality parameter A and scale σ, i.e., $M \sim \mathrm{Rice}(A,\sigma)$, see Appendix A.

The fundamental inconvenience of modeling Rician distributed data is the signal dependence of the variance which is given by:

$$\mathrm{Var}\{M|A,\sigma\} = A^2 + 2\sigma^2 - \frac{\pi\sigma^2}{2}\,{}_1F_1^2\left(-\frac{1}{2};1;-\frac{A^2}{2\sigma^2}\right), \tag{B.4}$$

where ${}_1F_1(\cdot;\cdot;\cdot)$ denotes the confluent hypergeometric function of the first kind.

Our goal here is to change the signal-dependent nature of the variance to a signal-independent one. Specifically, we are interested in a function $f_{\mathrm{stab}}\colon \mathbb{R} \mapsto \mathbb{R}$, which transforms the Rician RV to another RV with a constant variance:

$$\mathrm{Var}\{f_{\mathrm{stab}}(M)\} = 1.$$

Moreover, the new RV $f_{\mathrm{stab}}(M)$ should not depend on the noncentrality parameter A anymore [24].

In [81], the asymptotic stabilizer for Rician distributed RV is derived from Eq. (B.3) and the approximation of the conditional variance for large values of A was derived as:

$$f_{\mathrm{stab}}(M|\sigma) = \sqrt{\frac{M^2}{\sigma^2} - \frac{1}{2}} + a, \quad a \in \mathbb{R}, \tag{B.5}$$

where $M \geq \frac{\sqrt{2}}{2}\sigma$ and $a \in \mathbb{R}$ is an arbitrary constant.

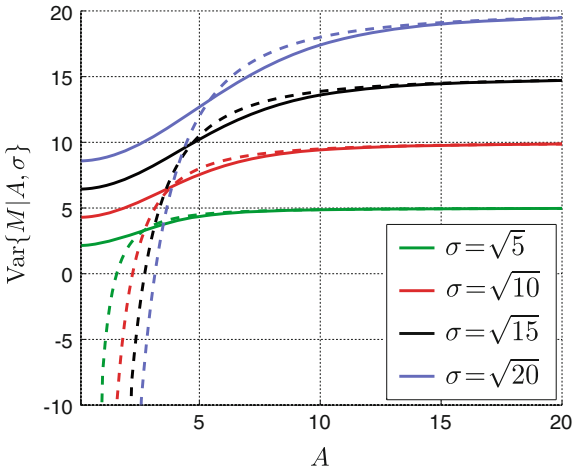

Fig. B.1 The conditional variance of Rician RV $\mathrm{Var}\{M|A,\sigma\}$ for different values of σ. The *solid lines* present the theoretical variance of Eq. (B.4), while *dashed lines* show the approximation of the conditional variance for larger values of A of Eq. (B.6)

The conditional variance $\mathrm{Var}\{M|A,\sigma\}$ used in the derivation procedure in Eq. (B.3) is given by the following approximation:

$$\mathrm{Var}\{M|A,\sigma\} \approx \sigma^2 - \frac{\sigma^4}{2A^2}. \tag{B.6}$$

In Fig. B.1, the approximation is shown for different values of σ, where the convergence of the approximation is shown as $A \to \infty$. This approximation makes feasible the calculation of a stabilizing transformation for higher SNR levels. However, the approximation applied is no longer valid for lower SNRs (i.e., SNR < 5). To handle low SNRs properly, Foi resorts to numerical models of the stabilizer f obtained from a direct optimization procedure [80]. The optimization procedure incorporates terms accounting for the accuracy of stabilization, smoothness, "convergence" of f to Eq. (B.5) as M approaches $M_{\max}$ and the closeness of the inverse transformation to the Rician ML estimate of the parameter A. The cost function to be optimized is defined as follows:

$$\begin{aligned} F(f) = &\int_0^{A_{\max}} \left(\mathrm{std}\{f(M)|\widetilde{A},1\}-1\right)^2 d\widetilde{A} + \lambda_{\mathrm{smooth}} \int_0^{M_{\max}} \left(\frac{d^2 f}{d\widetilde{M}^2}\right)^2 d\widetilde{M} \\ &+ \lambda_{\mathrm{asympt}} \int_0^{M_{\max}} \frac{1}{(M_{\max}-\widetilde{M}+\epsilon)^4} \left(f(\widetilde{M}) - f_{\mathrm{stab}}(\widetilde{M}|1)\right)^2 d\widetilde{M} \\ &+ \lambda_{\mathrm{inverse}} \int_0^{M_{\max}} \left(\mathcal{V}_f(f(\widetilde{M})) - \widehat{A_{\mathrm{ML}}}(\widetilde{M})\right)^2 d\widetilde{M}, \end{aligned} \tag{B.7}$$

where: $\mathrm{std}\{f(M)|\widetilde{A},1\}$ is the standard deviation of the stabilized data M by function f; $\epsilon = 2.0 \times 10^{-16}$ is used to ensure the well-posedness of the solution; $\mathcal{V}_f$: $E\{f(M)|A,1\} \to A$ is the exact unbiased inverse for the estimation of A,

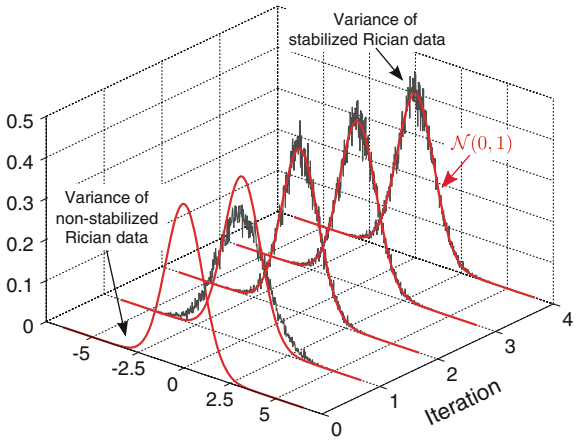

Fig. B.2 The results of the iterative stabilization scheme of Eq. (B.8) for stationary Rician distribution. The variance of the stabilized Rician data approximately follows a standard normal distribution $\mathcal{N}(0, 1)$

where $E\{f(M)|A, 1\}$ is the conditional expectation; $\widehat{A_{\mathrm{ML}}}$ is the Rician ML estimate obtained from a single sample M as the solution of the equation $\frac{M}{A}\frac{I_1(AM)}{I_0(AM)} = 1$ for $M > \sqrt{2}$ and $\widehat{A_{\mathrm{ML}}} = 0$ for $M \leq \sqrt{2}$; $\lambda_{\mathrm{smooth}} \geq 0$, $\lambda_{\mathrm{asympt}} \geq 0$, $\lambda_{\mathrm{inverse}} \geq 0$ are the penalty parameters of different factors in the cost function in Eq. (B.7).

Note that the cost function shown in Eq. (B.7) just considers a finite range of the parameters A (i.e., $A \in [0, A_{\max}]$) and $\sigma = 1$. Additionally, the variable M is considered to be in the range $[0, M_{\max}]$, so values over $M_{\max}$ are discarded due to the exponential decay of the Rician PDF.

The numerically precalculated function $f(M)$ along with the asymptotic stabilizer $f_{\mathrm{stab}}(M)$, Eqs. (B.7) and (B.5), are iteratively applied turning the random variable M into a standard AWGN component (see Fig. B.2). The iterative scheme is applied as follows:

$$\begin{cases} \widehat{\sigma}_1 = \mathfrak{C}\{M\}, \\ \widehat{\sigma}_{k+1} = \widehat{\sigma}_k \mathfrak{C}\{f_{\widehat{\sigma}_k}(M)\} \quad \text{with} \quad k \geq 1, \end{cases} \tag{B.8}$$

where $f_{\widehat{\sigma}_k}$ is the VST with the noise level parameter $\widehat{\sigma}_k$ and $\mathfrak{C}\{\cdot\}$ is an estimator of standard deviation, e.g., MAD estimator, see Eq. (6.9).

The approach is computationally intensive since each iteration requires the estimation of σ. Although the method is acceptable for single-coil systems, as it was originally proposed, the estimation of the parameter σ locally leads to significant under- or over-estimations due to a small number of samples used by the MAD estimator. Thus, a potential generalization of Foi's approach may lead to a biased estimator of σ, especially near edges and tissue transitions. For that reason, the Rician data is further incorrectly stabilized.

B.1.2 Variance Stabilization for All SNRs

In [179] authors presented a transformation scheme inspired in the VST derived from Foi that overcomes the main problems of conventional stabilizers for Rician distributed data:

1. It does not need an iterative scheme to estimate the parameter σ.
2. It stabilizes robustly the data for the whole range of SNRs.

This proposal requires an additional parameter to be estimated: the local SNR. Though the inclusion of an additional parameter in the derivation of the stabilizer could seem an inconvenience, we will show that both the initialization of σ and the estimation of the SNR per pixel can be efficiently achieved avoiding the main problems of other solutions. Besides, note that strictly speaking the VST approach tries to provide a transformation that does not depend on the central parameter A. That was accomplished in the asymptotic case by approximating the variance of M in Eq. (B.6) for high SNR values. Note, however, that a stabilization function based on the asymptotic approach that also deals with lower SNRs needs the inclusion of certain parameters accounting for the SNR level in which the random variable M is defined. Thus, the stabilization of M for all SNRs will be accomplished by relaxing the original definition of stabilizing function proposed by Bartlett [24], where the transformation was not just limited to provide a constant variance but also to be independent of the changes in the mean level (in this case the central parameter A). The following derivation will relax this strong constraint assuming that both parameters σ and A can be roughly approximated in order to provide a stabilization transformation that generalizes the asymptotic approach to lower SNRs.

The generalization of stabilizing transformation is derived from the parametrization of the asymptotic VST of Eq. (B.5) using two parameters $\alpha, \beta \in \mathbb{R}$ as follows:

$$f_{\text{stab}}(M|\sigma, \alpha, \beta) = \sqrt{\max\left\{\alpha^2 \frac{M^2}{\sigma^2} - \beta,\ 0\right\}} + a, \quad a \in \mathbb{R}, \tag{B.9}$$

where the operator $\max\{\cdot, \cdot\}$ avoids a negative argument of the square root function. Note that for $(\alpha, \beta) = (1, 0.5)$ the parametrized Eq. (B.9) becomes the asymptotic one.

In order to cope with different behaviors of the stabilizer, the parameters α and β should be tuned accordingly to the SNR of M. This can be efficiently achieved by using a numerical optimization procedure providing α and β as a function of the SNR with the following optimization criterion:

$$\left(\alpha_{\text{opt}}, \beta_{\text{opt}}\right) = \underset{\alpha,\beta\in\mathbb{R}}{\arg\min}\ J\left(f_{\text{stab}}(M|\sigma, \alpha, \beta)\right), \tag{B.10}$$

with $J: \mathbb{R}^2 \mapsto \mathbb{R}$ being a cost function to be minimized:

$$\begin{aligned} J\left(f_{\text{stab}}(M|\sigma,\alpha,\beta)\right) = \lambda_1 \cdot \varphi(1 - \text{Var}\left\{f_{\text{stab}}(M|\sigma,\alpha,\beta)\right\}) \\ + \lambda_2 \cdot \varphi(\text{Skewness}\{f_{\text{stab}}(M|\sigma,\alpha,\beta)\}) \\ + \lambda_3 \cdot \varphi(\text{ExcessKurtosis}\{f_{\text{stab}}(M|\sigma,\alpha,\beta)\}), \end{aligned} \tag{B.11}$$

where the weighting parameters meet the condition $\lambda_1+\lambda_2+\lambda_3 = 1$ and $\varphi: \mathbb{R} \to \mathbb{R}$ is a nonnegative convex function, e.g., $\varphi(x) = x^2$.

The components of Eq. (B.11) can be written in terms of the rth raw moments of the $f_{\text{stab}}-$transformed Rician RV as:

$$\begin{aligned} \text{Var}\left\{f_{\text{stab}}(M|\sigma,\alpha,\beta)\right\} &= m_2 - m_1^2, \\ \text{Skewness}\left\{f_{\text{stab}}(M|\sigma,\alpha,\beta)\right\} &= \frac{m_3 - 3m_1m_2 + 2m_1^3}{(m_2 - m_1^2)^{\frac{3}{2}}}, \\ \text{ExcessKurtosis}\left\{f_{\text{stab}}(M|\sigma,\alpha,\beta)\right\} &= \frac{m_4 - 4m_1m_3 + 6m_1^2m_2 - 3m_1^4}{(m_2 - m_1^2)^2} - 3, \end{aligned}$$

where rth raw moment, m_r, for the transformed Rician distribution is given by:

$$\begin{aligned} E\left\{f_{\text{stab}}^r(M|\sigma,\alpha,\beta)\right\} &= \int_0^\infty f_{\text{stab}}^r(\widetilde{M}|\sigma,\alpha,\beta)\, p(\widetilde{M}|A,\sigma)\, d\widetilde{M} \\ &= \int_0^\infty f_{\text{stab}}^r(\widetilde{M}|\sigma,\alpha,\beta)\, \frac{\widetilde{M}}{\sigma^2} \exp\left(-\frac{\widetilde{M}^2 + A^2}{2\sigma^2}\right) I_0\left(\frac{\widetilde{M}A}{\sigma^2}\right) d\widetilde{M} \end{aligned} \tag{B.12}$$

The cost function of Eq. (B.11) favors a unitary variance, zero skewness and zero excess kurtosis,[1] enforcing the desired Gaussian behavior of the transformed RV following the same philosophy as in [24].

As an illustration, the numerical optimization was carried out for $\sigma = 1$ and logarithmically increasing A between 0.001 and 20. The adaptive Gauss–Kronrod quadrature was used to calculate the moments shown in Eq. (B.12) over the interval $[0,\ 30]$, whereas the Nelder–Mead optimization method was applied for the optimization problem.

The results of the optimization procedure for $(\lambda_1, \lambda_2, \lambda_3) = (0.998, 0.001, 0.001)$ in terms of SNR ($\text{SNR} = A/\sigma$) are shown in Fig. B.3, and a comparison of the standard deviations of nonstabilized and stabilized Rician data for different configurations of parameters is also shown in Fig. B.4. For $(\alpha, \beta) = (1, \beta_{\text{opt}})$, the accuracy of the variance-stabilizing procedure outperformed the asymptotic stabilizer $(\alpha, \beta) = (1, 0.5)$. However, the solution is still not acceptable for low SNRs ($\text{SNR} < 1.171$). Substantial improvements can be observed simultaneously

[1] The excess kurtosis is defined as $\text{ExcessKurtosis}\{X\} = \text{Kurtosis}\{X\} - 3$. Note that the kurtosis of a Gaussian RV equals three.

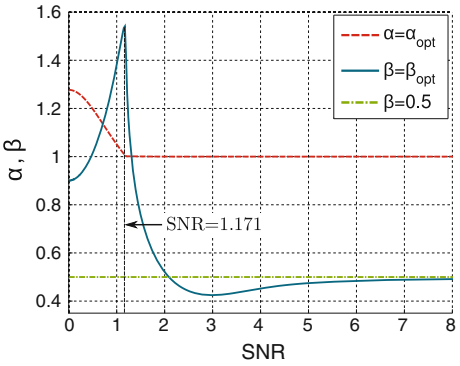

Fig. B.3 (Optimized parameters α_{opt} and β_{opt} of Eq. (B.11) in terms of SNR for $(\lambda_1, \lambda_2, \lambda_3) = (0.998, 0.001, 0.001)$

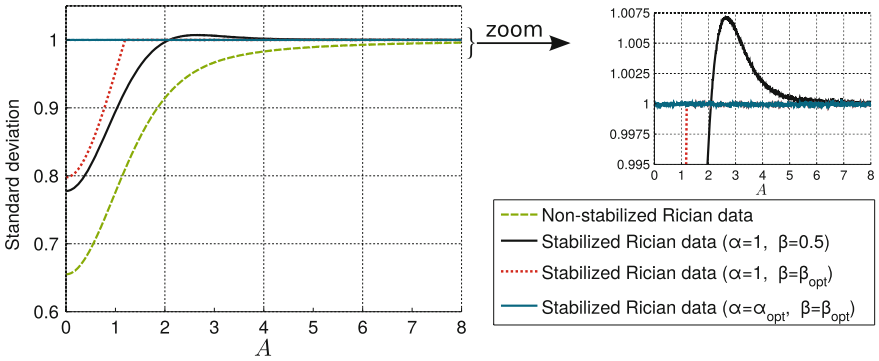

Fig. B.4 Comparison of standard deviations between nonstabilized Rician distributed data and the stabilized ones using different parameters α and β. *Right* zoom to the area of interest

applying the optimized pair of the parameters $\alpha_{\text{opt}}, \beta_{\text{opt}}$. The results obtained from the proposed parametric VST are then compared to Foi's models A and B (Fig. B.5). Note that the parametric form of the VST efficiently achieved the stabilization of the Rician RV for the whole range of SNRs.

One of the advantages of this parametric approach is that the stabilization of the data is noniterative and, thus, it is not computationally expensive. Additionally, its suitability for different SNRs allows this formulation to be applied in the case of non-stationary noise. On the other hand, the transformation f_{stab} needs a prior noise map $\sigma_0(\mathbf{x})$ and the local SNR of the image SNR($\mathbf{x}$). Many methods have been described in the literature for this purpose and some of them are introduced in Chaps. 6–11.

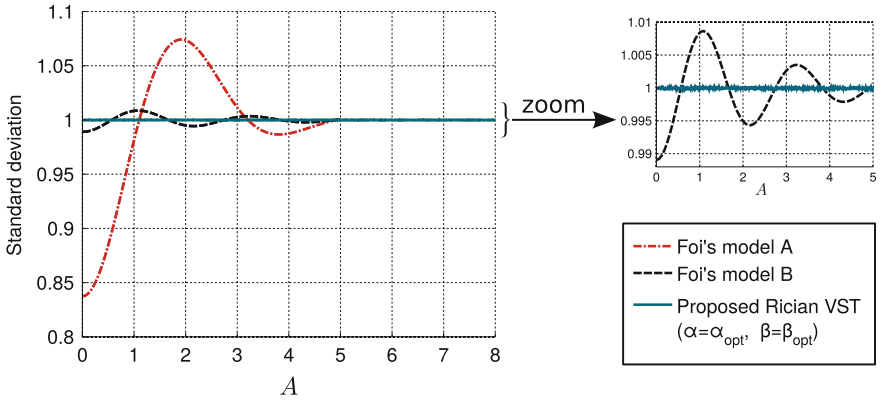

Fig. B.5 Standard deviation of the variance-stabilizing parametric approach $f_{\text{stab}}(M|\sigma, \alpha_{\text{opt}}, \beta_{\text{opt}})$ compared to the two stabilizers proposed by Foi with parameters: **a** $(\lambda_{\text{asympt}}, \lambda_{\text{smooth}}, \lambda_{\text{inverse}}) = (1, 10^{-2}, 10^{-1/2})$, **b** $(\lambda_{\text{asympt}}, \lambda_{\text{smooth}}, \lambda_{\text{inverse}}) = (1, 10^{-4}, 0)$. *Right* zoom to the area of interest

B.2 VST for nc-χ Distributed Data

B.2.1 Asymptotic Stabilizer

We are now interested in a function $f_{\text{stab}}: \mathbb{R} \to \mathbb{R}$, which stabilizes the variance of nc-χ distributed random variable M_T.

The main issue when stabilizing the variance of nc-χ data is the functional dependence of the variance with the mean and the number of coils L. Since M_T does not have a closed form for the expectation operator $E\{M_T\}$ (see Appendix A), in [180] authors propose the use of the squared random variable M_T^2 instead, which follows a nc-χ^2 distribution. Therefore, the odd raw moments can be expressed in closed-form expressions and consequently they are computationally tractable functions.

The expectation and the variance of M_T^2 are:

$$E\{M_T^2\} = A_T^2 + 2L\sigma^2, \tag{B.13}$$

$$\text{Var}\{M_T^2\} = 4A_T^2\sigma^2 + 4L\sigma^4, \tag{B.14}$$

where M_T is the CMS, σ is the underlying noise level, L is the number of receiver coils and A_T is the noise-free signal. Note that σ and L can be replaced by their effective equivalents σ_{eff} and L_{eff} if needed, see Chap. 3.

The starting point to derive the VST is the result in Eq. (B.3) that, for nc-χ^2, reads:

$$f_{\text{stab}}(M_T^2|A_T, \sigma, L) = \int^{M_T^2} \frac{1}{\sqrt{\text{Var}\{M_T^2|z, \sigma, L\}}}\, dz, \tag{B.15}$$

where $\mathrm{Var}\{M_T^2|z,\sigma,L\}$ is the conditional variance of nc-χ^2 distributed RV. This conditional variance is derived from the values in Eqs. (B.13) and (B.14):

$$\mathrm{Var}\{M_T^2\} = 4\sigma^2\left(E\{M_T^2\} - L\sigma^2\right). \tag{B.16}$$

If we denote $\mu_2 = E\{M_T^2\}$, we can rewrite Eq. (B.16) as the conditional variance of M_T^2:

$$\mathrm{Var}\{M_T^2|\mu_2,\sigma,L\} = 4\sigma^2\left(\mu_2 - L\sigma^2\right), \tag{B.17}$$

and then, the integral in Eq. (B.15) reads:

$$f_{\mathrm{stab}}(M_T^2|A_T,\sigma,L) = \frac{1}{2\sigma}\int^{M_T^2}\frac{1}{\sqrt{\mu_2 - L\sigma^2}}\,d\mu_2. \tag{B.18}$$

Finally, the stabilization function for nc-χ^2 RVs becomes [180]:

$$f_{\mathrm{stab}}(M_T^2|\sigma,L) = \frac{1}{\sigma}\sqrt{M_T^2 - L\sigma^2} = \sqrt{\frac{M_T^2}{\sigma^2} - L}. \tag{B.19}$$

Note that the formula in Eq. (B.19) is not properly the variance stabilizer for nc-χ RVs, but for nc-χ^2 RVs. This way, it does not converge to the Rician case in Eq. (B.19) when $L = 1$, as it should be for the nc-χ case.

We will denote the stabilizer defined in Eq. (B.18) as the asymptotic stabilizer since its convergence to a Gaussian distribution is guaranteed as $\mathrm{SNR} \to \infty$.

B.2.2 Robust Numerical Model for All SNRs

Due to the simplifications implicit in the transformation, the asymptotic model previously defined does not optimally work for low SNRs, see the example in Fig. B.6. To cope with this problem, Pieziak [180] proposed a robust numerical model, which improves the accuracy of VST for low SNRs, while keeping the properties of asymptotic transformation for high SNRs. To that end, Eq. (B.19) must be redefined using two extra parameters α and β:

$$f_{\mathrm{stab}}(M_T^2|\sigma,L,\alpha,\beta) = \frac{1}{\sigma}\sqrt{\max\{\alpha^2 M_L^2 - \beta L\sigma^2,\ 0\}}. \tag{B.20}$$

where the maximum operator is introduced to avoid a negative value under the square root sign. These parameters must be tuned for each SNR, defined as $\mathrm{SNR} = A_T/\sqrt{L\sigma^2}$. For this purpose, a numerical optimization procedure as the one defined in Eq. (B.10) must be carried out.

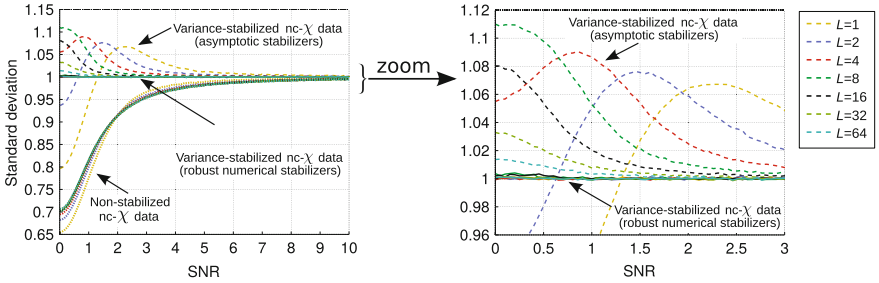

Fig. B.6 Comparison of standard deviations in terms of SNR $= A_T/\sqrt{L\sigma^2}$ between nonstabilized nc-χ data (*dotted lines*), variance-stabilized nc-χ data (*dashed lines*) and the robust numerical model (*solid lines*) for different number of receiver coils L. *Right* the zoomed figure for SNR $\in [0, 3]$

An example of the stabilization with optimal parameters is shown in Fig. B.6. The calculation of the raw moments was done with the adaptive Gauss–Kronrod quadrature over the interval [0, 800]. The asymptotic VST works efficiently for high SNRs, whereas the numerical approach stabilizes the data in the whole range of SNRs for all the cases considered. Note that the accuracy of the asymptotic model increases with increasing number of receiver coils.

Appendix C
Data Sets Used in the Experiments

C.1 Synthetic Data Sets

Single Slices

Four different slices MR slices from BrainWeb simulated database [57] at different transverse planes (T_1-, T_2- and PD-weighted MR data) are considered, all with intensity nonuniformity INU $= 0\,\%$. The data is free of noise, the background areas are set to zero, the slice thickness is 1 mm and the intensity range normalized to [0–255], see Fig. C.1a–d. For the sake of reference, the average intensity value in image in Fig. C.1d for the white matter is 158, for the gray matter is 105, for the cerebrospinal fluid 36 and 0 for the background.

Multi-Coil Simulation

In order to simulate synthetic multi-coil data the different synthetic slices in Fig. C.1 are used. The whole simulation scheme is depicted in Fig. C.2: an $L-$coil system is simulated using an artificial sensitivity map coded for each coil so that

$$A_T^2(\mathbf{x}) = \sum_{l=1}^{L} |A_l(\mathbf{x})|^2 = A_0(\mathbf{x}),$$

with $A_0(\mathbf{x})$ the original slice and $A_l(\mathbf{x})$ the simulation at lth coil. $A_l(\mathbf{x})$ is defined as the product of $A_0(\mathbf{x})$ with the sensitivity map of the lth coil:

$$A_l(\mathbf{x}) = C_l(\mathbf{x}) \cdot A_0(\mathbf{x}), \quad l = 1, \ldots, L$$

S. Aja-Fernández and G. Vegas-Sánchez-Ferrero,
Statistical Analysis of Noise in MRI, DOI 10.1007/978-3-319-39934-8

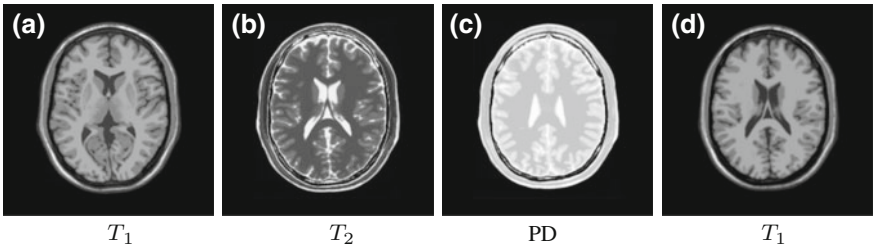

Fig. C.1 Synthetic data set used for the performance evaluation, from the BrainWeb database. **a** T_1. **b** T_2. **c** PD. **d** T_1

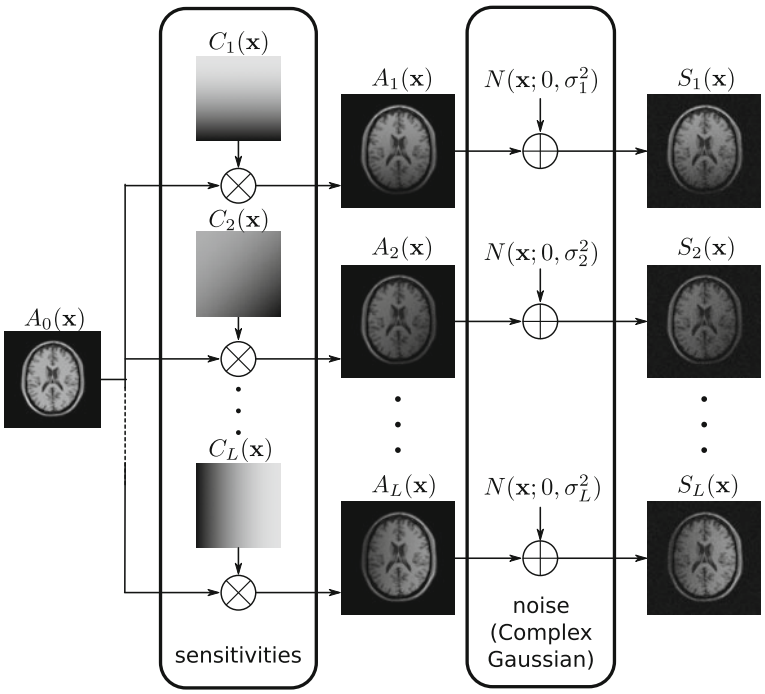

Fig. C.2 Scheme of multi-coil simulation using a synthetic slice and L synthetic sensitivity maps

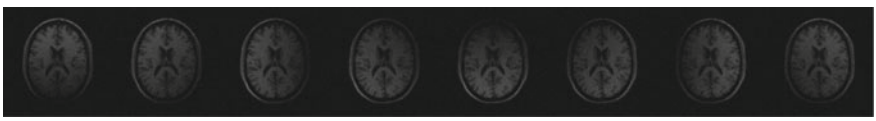

Fig. C.3 Synthetic 8-coil acquisition used for the multi-coil experiments

Fig. C.4 Synthetic sensitivity map created for the experiments

An illustration for the original slice in Fig. C.1d is shown in Fig. C.3, using the sensitivity map depicted in Fig. C.4. This configuration is equivalent to a set of sensitivities $C_l(\mathbf{x})$ so that:

$$\sum_{l=1}^{L} |C_l(\mathbf{x})|^2 = 1,$$

in all points. In order to simulate noisy acquisitions, images $A_l(\mathbf{x})$ are corrupted with complex Gaussian noise in each coil. Depending on the experiment, correlation between coils can be considered or not.

C.2 Real MRI Data Sets

Single-Coil

Data set 1: A 2D axial section of a brain, acquired using a General Electric Signa 1.5 T scanner, T_1-weighted slice, TR = 6 ms, TE = 1.588 ms, and flip angle = 15, see Fig. C.5a. 160 realizations of the same slice were considered, in order to perform statistical analysis over the data. The raw complex data is available.

Data set 2: A T_2 slice from the baseline of a brain DTI acquisition, scanned in a 1.5T GE SIGNA scanner, 256×256, 16 bits, slick thickness 5 mm, acquired with EPI, TR = 10000, TE = 80.9, NEX = 8, flip angle = 90, see Fig. C.5b.

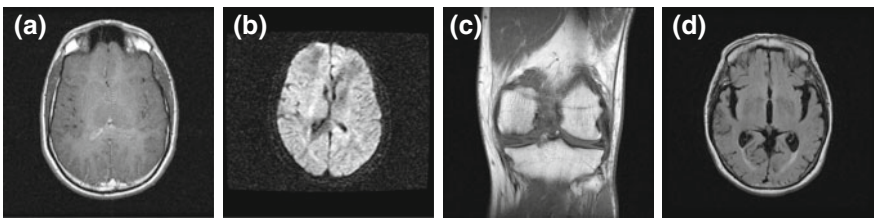

Fig. C.5 The real data sets considered for illustration in this chapter. They all have been acquired in 1.5 T scanners with single-coil acquisitions

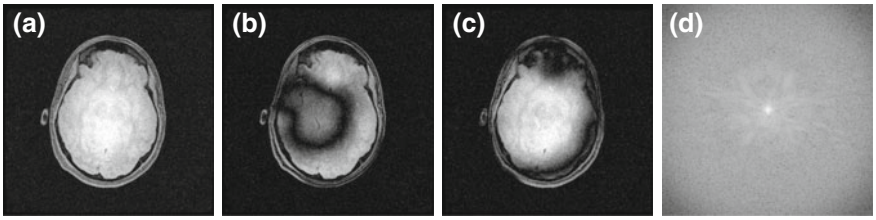

Fig. C.6 Data set 5: Raw data from an 1.5 T scanner with single-coil acquisitions

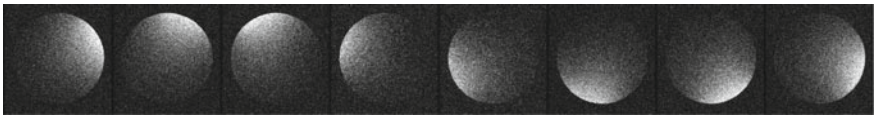

Fig. C.7 Data set 6: Multi-coil slice of an 8-coil acquisition of a doped ball phantom

Data set 3: A T_1 FSE acquisition of a knee, scanned in a 1.5T GE SIGNA scanner, 512×512, 16 bits, slick thickness 5 mm, TR = 900, TE = 12.4440, NEX = 1, flip angle = 90, see Fig. C.5c.

Data set 4: A T_2 FLAIR slice from a brain DTI acquisition, scanned in a 1.5T GE SIGNA scanner, 512×512, 16 bits, slick thickness 5 mm, acquired with EPI, TR = 8002, TE = 88.4520, NEX = 1, flip angle = 90, see Fig. C.5d.

Data set 5: An axial, single-coil multi-echo spoiled gradient echo volume, acquired in a GE MR750 using a single channel quadrature T/R head coil with the IDEAL3D GE protocol, Axial, FOV = 28×28cm, slice thickness 3mm, frequency direction A/P, TR = 20.1, 1 shot, FA 9, ETL 6, 256×256 matrix, nex = 1, rBW = +/−125, see Fig. C.6. The **k**-space is available, and from there, the complex signal $s(\mathbf{x})$ is reconstructed.

Raw Fully Sampled Multi-Coil Data

Data set 6: A doped ball scanned in an 8-channel head coil on a GE Signa 1.5T EXCITE 12m4 scanner with FGRE Pulse Sequence, matrix size 128×128, TR/TE = 8.6/3.38, FOV = 21×21 cm, see Fig. C.7. 100 realizations of the same slice were considered, in order to perform statistical analysis over the data. The raw complex data is available.

Data set 7: A slice of a brain acquisition from an 8 coil GE Signa 1.5 Tesla EXCITE 11m4 scanner, FSE Pulse Sequence, TR = 500 ms, TE = 13.8 ms, matrix size = 256×256, FOV = 20×20 cm, slick thickness = 5 mm, see Fig. C.8.

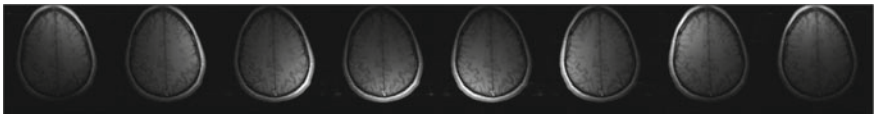

Fig. C.8 Data set 7: Multi-coil slice acquired in a 1.5 T scanner with 8-coil acquisition

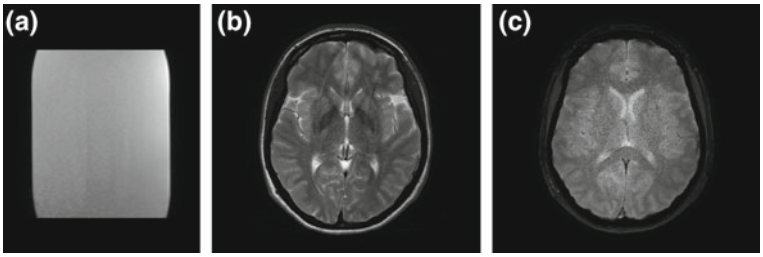

Data set 8 Data set 9 Data set 10

Fig. C.9 Real Data sets acquired with SENSE: **a** T_1-weighted TFE SENSE physical phamtom ($r = 2$); **b** T_2 weighted TSE SENSE MR data ($r = 4$); **c** T_2 weighted FFE SENSE MR data ($r = 4$)

Real SENSE Acquisitions

Data set 8: A SENSE reconstruction of a physical phantom acquisition. Twenty repetitions of a T_1-weighted scan of a doped cylinder phantom were performed using Philips Achieva 3.0T TX device provided with a 32-channel coil system using Turbo Field Echo (TFE) sequence, volume size $224 \times 224 \times 59$, TR $=$ 5.264 ms/TE $=$ 2.569 ms, slice thickness 3.20 mm, and reduction factor $r = 2$. Figure C.9a.

Data sets 9 and 10: Real SENSE MR brain data: two T_2-weighted scans of the brain in transverse planes were acquired by Philips Achieva 3.0T TX scanner provided with the 32-channel head coil. The first data set was acquired using Fast Field Echo (FFE) sequence, volume size $240 \times 180 \times 161$, TR $=$ 3000 ms/TE $=$ 80 ms, slice thickness 3.20 mm. The second one was obtained using Turbo Spin Echo (TSE). The **k**-space was subsampled by the reduction factor $r = 4$ for both acquisitions. Figure C.9b, c.

Other Data Sets

In Chap. 5 some data sets are used for illustration of the advantages of filtering. Results were directly taken from the cited publications and no further processing has been done over those data sets.

References

1. Ahn, C., Song, Y., Park, D.: Adaptive template filtering for signal-to-noise ratio enhancement in magnetic resonance imaging. IEEE Trans. Med. Imaging **18**(6), 549–556 (1999)
2. Aja-Fernández, S., Alberola-López, C., Westin, C.F.: Signal LMMSE estimation from multiple samples in MRI and DT-MRI. In: Proceedings of MICCAI 07. Lecture Notes on Computer Science, vol. 4792, pp. 368–375 (2007)
3. Aja-Fernández, S., Alberola-López, C., Westin, C.F.: Noise and signal estimation in magnitude MRI and Rician distributed images: a LMMSE approach. IEEE Trans. Image Process. **17**(8), 1383–1398 (2008)
4. Aja-Fernández, S., Garcia-Martin, D., Tristán-Vega, A., Vegas-Sánchez-Ferrero, G.: Improving GRAPPA reconstruction by frequency discrimination in the ACS lines. Int. J. Comput. Assist. Radiol. Surg. **10**(10), 1699–1710 (2015)
5. Aja-Fernández, S., de Luis Garcia, R., Alberola-Lopez, C., Hernando, D.: Quantitative diffusion MRI in the presence of noise: effects of filtering and fitting technique. In: Quantitative Medical Imaging, pp. QTu2G–2. Optical Society of America (2013)
6. Aja-Fernández, S., Martín, D.G., Tristán-Vega, A., Vegas-Sánchez-Ferrero, G.: Improving GRAPPA reconstruction by frequency discrimination in the ACS lines. Int. J. Comput. Assist. Radiol. Surg. **10**(10), 1699–1710 (2015)
7. Aja-Fernández, S., Niethammer, M., Kubicki, M., Shenton, M.E., Westin, C.F.: Restoration of DWI data using a Rician LMMSE estimator. IEEE Trans. Med. Imag. **27**(10), 1389–1403 (2008)
8. Aja-Fernández, S., Pieciak, T., Vegas-Sanchez-Ferrero, G.: Spatially variant noise estimation in MRI: a homomorphic approach. Med. Imag. Anal. **20**, 184–197 (2015)
9. Aja-Fernández, S., Tristán-Vega, A.: Influence of noise correlation in multiple-coil statistical models with sum of squares reconstruction. Magn. Reson. Med. **67**(2), 580–585 (2012)
10. Aja-Fernández, S., Tristán-Vega, A., Alberola-López, C.: Noise estimation in single- and multiple-coil magnetic resonance data based on statistical models. Magn. Reson. Imag. **27**, 1397–1409 (2009)
11. Aja-Fernández, S., Tristán-Vega, A., Brion, V.: Effective noise estimation and filtering from correlated multiple-coil MR sdata. Magn. Reson. Imaging **31**(2), 272–285 (2013)
12. Aja-Fernández, S., Tristán-Vega, A., Hoge, W.S.: Statistical noise analysis in GRAPPA using a parametrized non-central chi approximation model. Magn. Reson. Med. **65**(4), 1195–1206 (2011)
13. Aja-Fernández, S., Vegas-Sanchez-Ferrero, G.: Blind estimation of spatially variant noise in GRAPPA MRI. In: 2015 IEEE International Symposium on Biomedical Imaging, ISBI. Brooklyn (2015)

S. Aja-Fernández and G. Vegas-Sánchez-Ferrero,
Statistical Analysis of Noise in MRI, DOI 10.1007/978-3-319-39934-8

14. Aja-Fernández, S., Vegas-Sánchez-Ferrero, G., Martín-Fernández, M., Alberola-López, C.: Automatic noise estimation in images using local statistics. Additive and multiplicative cases. Image Vis. Comput. **27**(6), 756–770 (2009)
15. Aja-Fernández, S., Vegas-Sanchez-Ferrero, G., Tristán-Vega, A.: About the background distribution in MR data: a local variance study. Magn. Reson. Imaging **28**, 739–752 (2010)
16. Aja-Fernández, S., Vegas-Sánchez-Ferrero, G., Tristán-Vega, A.: Noise estimation in parallel MRI: GRAPPA and SENSE. Magn. Reson. Imaging **32**(3), 281–290 (2014)
17. Alexander, D.C.: A general framework for experiment design in diffusion MRI and its application in measuring direct tissue-microstructure features. Magn. Reson. Med. **60**(2), 439–448 (2008)
18. Alvarez, L.: Images and PDE's. In: Lecture Notes in Control and Information Sciences, vol. 219. Springer, London (1996)
19. Andersson, J.: Maximum a posteriori estimation of diffusion tensor parameters using a Rician noise model: why, how and but. NeuroImage **42**(4), 1340–1356 (2008)
20. Atkins, M.S., Mackiewich, B.T.: Fully automatic segmentation of the brain in MRI. IEEE Trans. Med. Imaging **17**(1), 98–107 (1998)
21. Awate, S.P., Whitaker, R.T.: Nonparametric neighborhood statistics for MRI denoising. Proceedings of International Conference on Information Processing in Medical Imaging **3565**, 677–688 (2005)
22. Awate, S.P., Whitaker, R.T.: Unsupervised, information-theoretic, adaptive image filtering for image restoration. Inf. Process. Med. Imaging **28**, 364–376 (2006)
23. Awate, S.P., Whitaker, R.T.: Feature-preserving MRI denoising: a nonparametric empirical Bayes approach. IEEE Trans. Med. Imaging **26**(9), 1242–1255 (2007)
24. Bartlett, M.S.: The use of transformations. Biometrics **3**(1), 39–52 (1947)
25. Basser, P., Pierpaoli, C.: Microstructural and physiological features of tissues elucidated by Quantitative-Diffusion-Tensor MRI. J. Magn. Reson. **111**(3), 209–219 (1996)
26. Basu, S., Fletcher, T., Whitaker, R.: Rician noise removal in diffusion tensor MRI. In: Medical Image Computing and Computer-Assisted Intervention–MICCAI 2006, pp. 117–125. Springer, Berlin (2006)
27. Beaulieu, N.C.: An infinite series for the computation of the complementary probability distribution function of a sum of independent ramdom variables and its application to the sum of Rayleigh random variables. IEEE Trans. Commun. **38**(9), 1463–1473 (1990)
28. Biswal, B., Deyoe, E.A., Hyde, J.S.: Reduction of physiological fluctuations in fMRI using digital filters. Magn. Reson. Med. **35**(1), 107–113 (1996)
29. Black, M.J., Sapiro, G., Marimont, D.H., Heeger, D.: Robust anisotropic diffusion. IEEE Trans. Image Process. **7**(3), 421–432 (1998)
30. Blaimer, M., Breuer, F., Mueller, M., Heidemann, R., Griswold, M., Jakob, P.: SMASH, SENSE, PILS, GRAPPA: how to choose the optimal method. Top Magn. Reson. Imaging **15**(4), 223–36 (2004)
31. Bloch, F.: Nuclear induction. Phys. Rev. **70**, 460–474 (1946)
32. Borrelli, P., Palma, G., Comerci, M., Alfano, B.: Unbiased noise estimation and denoising in parallel magnetic resonance imaging. In: International Conference on Acoustics, Speech, and Signal Processing (ICASSP), pp. 1230–1234 (2014)
33. Botev, Z.I., Grotowski, J.F., Kroese, D.P., et al.: Kernel density estimation via diffusion. Ann. Stat. **38**(5), 2916–2957 (2010)
34. Boulanger, J., Kervrann, C., Bouthemy, P., Elbau, P., Sibarita, J.B., Salamero, J.: Patch-based nonlocal functional for denoising fluorescence microscopy image sequences. IEEE Trans. Med. Imaging **29**(2), 442–454 (2010)
35. Breuer, F.A., Blaimer, M., Mueller, M.F., Seiberlich, N., Heidemann, R.M., Griswold, M.A., Jakob, P.M.: Controlled aliasing in volumetric parallel imaging (2D CAIPIRINHA). Magn. Reson. Med. **55**(3), 549–556 (2006)
36. Breuer, F.A., Kannengiesser, S.A., Blaimer, M., Seiberlich, N., Jakob, P.M., Griswold, M.A.: General formulation for quantitative G-factor calculation in GRAPPA reconstructions. Magn. Reson. Med. **62**(3), 739–746 (2009)

37. Brion, V.: Towards real-time diffusion imaging: noise correction and inference of the human brain connectivity. Ph.D. thesis, Université Paris-sud 11 École Doctorale Stits Neurospin, Cea, Paris, France (2013)
38. Brion, V., Kezele, I., Descoteaux, M., Mangin, J., Poupon, C.: Rician denoising dedicated to single-shell diffusion-weighted MR data using spherical harmonics: impact on fibre orientation distribution maps. ESMRMB **52**, 142–145 (2009)
39. Brion, V., Poupon, C., Riff, O., Aja-Fernández, S., Tristán-Vega, A., Mangin, J.F., Le Bihan, D., Poupon, F.: Parallel MRI noise correction: an extension of the lmmse to non central χ distributions. In: Medical Image Computing and Computer-Assisted Intervention–MICCAI 2011, pp. 226–233. Springer, Berlin (2011)
40. Brion, V., Poupon, C., Riff, O., Aja-Fernández, S., Tristán-Vega, A., Mangin, J.F., LeBihan, D., Poupon, F.: Parallel MRI noise correction: an extension of the LMMSE to non central Chi distributions. In: MICCAI 2011. Lecture Notes in Computer Science, vol. 6891, pp. 217–224 (2011)
41. Brown, R., Wang, Y., Spincemaille, P., Lee, R.F.: On the noise correlation matrix for multiple radio frequency coils. Magn. Reson. Med. **58**, 218–224 (2004)
42. Brummer, M., Mersereau, R., Eisner, R., Lewine, R.: Automatic detection of brain contours in MRI data sets. IEEE Trans. Med. Imaging **12**(2), 153–166 (1993)
43. Buades, A., Coll, B., Morel, J.: A review of image denoising algorithms, with a new one. Multiscale Model. Simul. **4**(2), 490–530 (2005)
44. Bydder, M., Larkman, D., Hajnal, J.: Generalized SMASH imaging. Magn. Reson. Med. **47**, 160–170 (2002)
45. Bydder, M., Larkman, D.J., Hajnal, J.V.: Combination of signals from array coils using image-based estimation of coil sensitivity profiles. Magn. Reson. Med. **47**(3), 539–548 (2002)
46. Casaseca-de-la-Higuera, P., Tristán-Vega, A., Aja-Fernández, S., Alberola-López, C., Westin, C.F., San-José-Estépar, R.: Optimal real-time estimation in diffusion tensor imaging. Magn. Reson. Imaging **30**(4), 506–517 (2012)
47. Catté, F., Lions, P., Morel, J., Coll, T.: Image selective smoothing and edge detection by nonlinear diffusion. SIAM J. Numer. Anal. **29**, 182–193 (1992)
48. Chang, L.C., Rohde, G.K., Pierpaoli, C.: An automatic method for estimating noise-induced signal variance in magnitude-reconstructed magnetic resonance images. Med. Imaging 2005: Image Process. **5747**(1), 1136–1142 (2005)
49. Chang, S., Kwon, Y., Yang, S.I., Kim, I.j.: Speech enhancement for non-stationary noise environment by adaptive wavelet packet. In: 2002 IEEE International Conference on Acoustics, Speech, and Signal Processing (ICASSP), vol. 1, pp. I–561–I–564 (2002)
50. Chang, Y., Liang, D., Ying, L.: Nonlinear GRAPPA: a kernel approach to parallel MRI reconstruction. Magn. Reson. Med. **68**(3), 730–740 (2012)
51. Chen, B., Hsu, E.W.: Noise removal in magnetic resonance diffusion tensor imaging. Magn. Reson. Med. **54**(2), 393–401 (2005)
52. Chen, Z., Zhang, J., Yang, R., Kellman, P., Johnston, L.A., Egan, G.F.: IIR GRAPPA for parallel MR image reconstruction. Magn. Reson. Med. **63**(2), 502–509 (2010)
53. Chernoff, H.: Estimation of the mode. Ann. Inst. Stat. Math. **16**(1), 31–41 (1964)
54. Chung, A.C.S., Noble, J.A.: Statistical 3D vessel segmentation using a Rician distribution. Proceedings of the 2nd MICCAI. Lecture Notes in Computer Science, vol. 1679, pp. 82–89. Springer, Berlin (1999)
55. Clarke, L., Velthuizen, R., Camacho, M., Heine, J., Vaidyanathan, M., Hall, L., Thatcher, R., Silbiger, M.: MRI segmentation: methods and applications. Magn. Reson. Imaging **13**(3), 343–368 (1995)
56. Clarke, R., Scifo, P., Rizzo, G., Dell'Acqua, F., Scotti, G., Fazio, F.: Noise correction on Rician distributed data for fibre orientation estimators. IEEE Trans. Med. Imaging **27**(9), 1242–1251 (2008)
57. Collins, D., Zijdenbos, A., Kollokian, V., Sled, J., Kabani, N., Holmes, C., Evans, A.: Design and construction of a realistic digital brain phantom. IEEE Trans. Med. Imaging **17**(3), 463–468 (1998)

58. Constantinides, C., Atalar, E., McVeigh, E.: Signal-to-noise measurements in magnitude images from NMR based arrays. Magn. Reson. Med. **38**, 852–857 (1997)
59. Coupé, P., Manjón, J.V., Gedamu, E., Arnold, D., Robles, M., Collins, D.L.: Robust Rician noise estimation for MR images. Med. Image Anal. **14**(4), 483–493 (2010)
60. Coupé, P., Yger, P., Prima, S., Hellier, P., Kervrann, C., Barillot, C.: An optimized blockwise non local means denoising filter for 3D magnetic resonance images. IEEE Trans. Med. Imaging **27**, 425–441 (2008)
61. Dabov, K., Foi, A., Katkovnik, V., Egiazarian, K.: Image denoising by sparse 3-D transform-domain collaborative filtering. IEEE Trans. Image Process. **16**(8), 2080–2095 (2007)
62. Delakis, I., Hammad, O., Kitney, R.I.: Wavelet-based de-noising algorithm for images acquired with parallel magnetic resonance imaging (MRI). Phys. Med. Biol. **52**(13), 3741 (2007)
63. DeLaPaz, R.L.: Echo-planar imaging. Radiographics **14**, 1045–1058 (1994)
64. Deng, L., Droppo, J., Acero, A.: Recursive estimation of nonstationary noise using iterative stochastic approximation for robust speech recognition. IEEE Trans. Speech Audio Process. **11**(6), 568–580 (2003)
65. Descoteaux, M., Wiest-Daesslé, N., Prima, S., Barillot, C., Deriche, R.: Impact of Rician adapted non-local means filtering on HARDI. In: Medical Image Computing and Computer-Assisted Intervention–MICCAI 2008, pp. 122–130. Springer, Berlin (2008)
66. DeVore, M.D., Lanterman, A.D., O'Sullivan, J.A.: ATR performance of a Rician model for SAR images. In: Proceedings of SPIE 2000, pp. 34–37. Orlando (2000)
67. Devroye, L.: Recursive estimation of the mode of a multivariate density. Can. J. Stat. **7**(2), 159–167 (1979)
68. Dietrich, O., Raya, J.G., Reeder, S.B., Ingrisch, M., Reiser, M.F., Schoenberg, S.O.: Influence of multichannel combination, parallel imaging and other reconstruction techniques on MRI noise characteristics. Magn. Reson. Imaging **26**, 754–762 (2008)
69. Dikaios, N., Punwani, S., Hamy, V., Purpura, P., Rice, S., Forster, M., Mendes, R., Taylor, S., Atkinson, D.: Noise estimation from averaged diffusion weighted images: can unbiased quantitative decay parameters assist cancer evaluation? Magn. Reson. Med. **71**(6), 2105–2117 (2014)
70. Ding, Y., Chung, Y.C., Simonetti, O.P.: A method to assess spatially variant noise in dynamic MR image series. Magn. Reson. Med. **63**(3), 782–789 (2010)
71. Dolui, S., Kuurstra, A., Michailovich, O.V.: Rician compressed sensing for fast and stable signal reconstruction in diffusion MRI. In: Haynor, D.R., Ourselin, S. (eds.) Medical Imaging 2012: Image Processing, vol. 8314. SPIE (2012)
72. Dolui, S., Kuurstra, A., Patarroyo, I.C.S., Michailovich, O.V.: A new similarity measure for non-local means filtering of MRI images. J. Vis. Commun. Image Represent. **24**(7), 1040–1054 (2013)
73. Donoho, D., Johnstone, I.: Ideal spatial adaptation by wavelet shrinkage. Biometrika **81**, 425–455 (1994)
74. Donoho, D.L.: De-noising by soft-thresholding. IEEE Trans. Inf. Theory **41**(3), 613–627 (1995)
75. Drumheller, D.: General expressions for Rician density and distribution functions. IEEE Trans. Aerosp. Electron. Syst. **29**(2), 580–588 (1993)
76. Edelstein, W., Glover, G., Hardy, C., Redington, R.: The intrinsic signal-to-noise ratio in NMR imaging. Magn. Reson. Med. **3**(4), 604–618 (1986)
77. Feng, Y., He, T., Feng, M., Carpenter, J.P., Greiser, A., Xin, X., Chen, W., Pennell, D.J., Yang, G.Z., Firmin, D.N.: Improved pixel-by-pixel MRI R2* relaxometry by nonlocal means. Magn. Reson. Med. **72**(1), 260–268 (2014)
78. Feng, Y., He, T., Gatehouse, P.D., Li, X.: Harith Alam, M., Pennell, D.J., Chen, W., Firmin, D.N.: Improved MRI R2* relaxometry of iron-loaded liver with noise correction. Magn. Reson. Med. **70**(6), 1765–1774 (2013)
79. Fillard, P., Pennec, X., Arsigny, V., Ayache, N.: Clinical DT-MRI estimation, smoothing, and fiber tracking with log-Euclidean metrics. IEEE Trans. Med. Imaging **26**(11), 1472–1482 (2007)

80. Foi, A.: Optimization of variance-stabilizing transformations. Preprint, 2009b **94** (2009)
81. Foi, A.: Noise estimation and removal in MR imaging: the variance-stabilization approach. In: IEEE International Symposium on Biomedical Imaging (ISBI), pp. 1809–1814 (2011)
82. Friman, O., Hennemuth, A., Peitgen, H.O.: A Rician-Gaussian mixture model for segmenting delayed enhancement MRI images. In: Proceedings of the 16th Scientific Meeting of the ISMRM, vol. 3, p. 1040 (2008)
83. Fujimoto, M., Nakamura, S.: Sequential non-stationary noise tracking using particle filtering with switching dynamical system. In: 2006 IEEE International Conference on Acoustics, Speech and Signal Processing, 2006. ICASSP 2006 Proceedings, vol. 1, pp. I–I (2006)
84. Gerig, G., Kbler, O., Kikinis, R., Jolesz, F.: Nonlinear anisotropic filtering of MRI data. IEEE Trans. Med. Imaging **11**(2), 221–232 (1992)
85. Glenn, G.R., Tabesh, A., Jensen, J.H.: A simple noise correction scheme for diffusional kurtosis imaging. Magn. Reson. Imaging **33**(1), 124–133 (2015)
86. Goossens, B., Pizurica, A., Philips, W.: Wavelet domain image denoising for non-stationary noise and signal-dependent noise. In: IEEE International Conference on Image Processing, pp. 1425–1428 (2006)
87. Griswold, M.A., Breuer, F., Blaimer, M., Kannengiesser, S., Heidemann, R.M., Mueller, M., Nittka, M., Jellus, V., Kiefer, B., Jakob, P.M.: Autocalibrated coil sensitivity estimation for parallel imaging. NMR Biomed. **19**(3), 316–324 (2006)
88. Griswold, M.A., Jakob, P.M., Heidemann, R.M., Nittka, M., Jellus, V., Wang, J., Kiefer, B., Haase, A.: Generalized autocalibrating partially parallel acquisitions (GRAPPA). Magn. Reson. Med. **47**(6), 1202–1210 (2002)
89. Gudbjartsson, H., Patz, S.: The Rician distribution of noisy MRI data. Magn. Reson. Med. **34**(6), 910–914 (1995)
90. Guleryuz, O.G.: Weighted averaging for denoising with overcomplete dictionaries. IEEE Trans. Image Process. **16**, 3020–3034 (2007)
91. Guo, L., Wu, Y., Liu, X., Li, Y., Xu, G., Yan, W.: Threshold optimization of adaptive template filtering for MRI based on intelligent optimization algorithm. In: 28th Annual International Conference of the IEEE Engineering in Medicine and Biology Society, 2006. EMBS'06, pp. 4763–4766. IEEE (2006)
92. Guo, W., Huang, F.: Adaptive total variation based filtering for MRI images with spatially inhomogeneous noise and artifacts. In: IEEE International Symposium on Biomedical Imaging: From Nano to Macro, 2009. ISBI'09, pp. 101–104 (2009)
93. Haldar, J.P., Wedeen, V.J., Nezamzadeh, M., Dai, G., Weiner, M.W., Schuff, N., Liang, Z.P.: Improved diffusion imaging through SNR-enhancing joint reconstruction. Magn. Reson. Med. **69**(1), 277–289 (2013)
94. Hansen, M.S., Inati, S.J., Kellman, P.: Noise propagation in region of interest measurements. Magn. Reson. Med. **73**(3), 1300–1308 (2015)
95. Harpen, M.: Noise correlations exist for independent RF coils. Magn. Reson. Med. **23**, 394–397 (1992)
96. Hayes, C., Roemer, P.B.: Noise correlations in data simultaneously acquired form multiple surface coil arrays. Magn. Reson. Med. **16**, 181–191 (1990)
97. He, L., Greenshields, I.: A nonlocal maximum likelihood estimation method for Rician noise reduction in MR images. IEEE Trans. Med. Imaging **28**(2), 165–172 (2009)
98. Healey, G.E., Kondepudy, R.: Radiometric CCD camera calibration and noise estimation. IEEE Trans. Pattern Anal. Mach. Intell. **16**(3), 267–276 (1994)
99. Healy, D.M., Weaver, J.B.: Two applications of wavelet transforms in magnetic resonance imaging. IEEE Trans. Inf. Theory **38**, 840–860 (1992)
100. Henkelman, R.: Measurement of signal intensities in the presence of noise in MR images. Med. Phys. **12**(2), 232–233 (1985)
101. Hennemuth, A., Seeger, A., Friman, O., Miller, S., Klumpp, B., Oeltze, S., Peitgen, H.O.: A comprehensive approach to the analysis of contrast enhanced cardiac MR images. IEEE Trans. Med. Imaging **27**(11), 1592–1610 (2008)

102. Henrichon, E., Fu, K.: On mode estimation in pattern recognition. In: Seventh Symposium on Adaptive Processes, vol. 7, p. 31 (1968)
103. Hirokawa, Y., Isoda, H., Maetani, Y.S., Arizono, S., Shimada, K., Togashi, K.: MRI artifact reduction and quality improvement in the upper abdomen with PROPELLER and prospective acquisition correction (PACE) technique. Am. J. Roentgenol. **191**(4), 1154–1158 (2008)
104. Hoge, W.S., Brooks, D.H., Madore, B., Kyriakos, W.E.: A tour of accelerated parallel MR imaging from a linear systems perspective. Concept. Magn. Reson. Part A **27A**(1), 17–37 (2005)
105. Hu, J., Beaulieu, N.C.: Accurate closed-form approximations to Ricean sum distributions and densities. IEEE Commun. Lett. **9**(2), 133–135 (2005)
106. Huang, F., Li, Y., Vijayakumar, S., Hertel, S., Duensing, G.R.: High-pass GRAPPA: an image support reduction technique for improved partially parallel imaging. Magn. Reson. Med. **59**(3), 642–649 (2008)
107. Immerkaer, J.: Fast noise variance estimation. Comput. Vis. Image Underst. **64**(2), 300–302 (1996)
108. Jezzard, P., LeBihan, D., Cuenod, C., Pannier, L., Prinster, A., Turner, R.: An investigation of the contribution of physiological noise in human functional MRI studies at 1.5 Tesla and 4 Tesla. In: Proceedings of the 12th Annual Meeting of SMRM, New York, p. 1392 (1993)
109. Jiang, L., Yang, W.: Adaptive magnetic resonance image denoising using mixture model and wavelet shrinkage. In: Proceedings of VIIth Digital Image Computing: Techniques and Applications, pp. 831–838. Sydney (2003)
110. Johnston, B., Atkins, M.S., Mackiewich, B., Anderson, M.: Segmentation of multiple sclerosis lesions in intensity corrected multispectral MRI. IEEE Trans. Med. Imaging **15**(2), 154–169 (1996)
111. Jonasson, L.: Segmentation of diffusion weighted MRI using the level set framework. Ph.D. thesis, École Polytechnique Fédérale de Lausanne, Laussane, Swiss (2005)
112. Jones, D.K., Basser, P.J.: squashing peanuts and smashing pumpkins: how noise distorts diffusion-weighted MR data. Magn. Reson. Med. **52**(5), 979–993 (2004)
113. Kay, S.M.: Fundamentals of Statistical Signal Processing: Estimation Theory. Prentice Hall, Englewood Cliffs (1993)
114. van Kempen, G.M.P., van Vliet, L.J.: Background estimation in nonlinear image restoration. J. Opt. Soc. Am. A **17**(3), 425–433 (2000)
115. Kim, S., Lim, H.: Fourth-order partial differential equations for effective image denoising. Electron. J. Differ. Equ. **17**, 107–121 (2009)
116. King, K., Moran, P.: A unified description of NMR imaging, data collection strategies and reconstruction. Med. Phys. **11**(1), 1–14 (1984)
117. Koay, C.G., Basser, P.J.: Analytically exact correction scheme for signal extraction from noisy magnitude MR signals. J. Magn. Reson. **179**, 317–322 (2006)
118. Koay, C.G., Özarslan, E., Basser, P.J.: A signal transformational framework for breaking the noise floor and its applications in MRI. J. Magn. Reson. **197**(2), 108–119 (2009)
119. Konstantinides, K., Natarajan, B., Yovanof, G.S.: Noise estimation and filtering using block-based singular value decomposition. IEEE Trans. Image Process. **6**(3), 479–483 (1997)
120. Krissian, K., Aja-Fernández, S.: Noise-driven anisotropic diffusion filtering of MRI. IEEE Trans. Image Process. **18**(10), 2265–2274 (2009)
121. Kruger, G., Glover, G.H.: Physiological noise in oxygenation-sensitive magnetic resonance imaging. Magn. Reson. Med. **46**, 1631–637 (2001)
122. Kurita, T., Otsu, N., Abdelmalek, N.: Maximum likelihood thresholding based on population mixture models. Pattern Recognit. **25**(10), 1231–1240 (1992)
123. Lam, F., Babacan, S.D., Haldar, J.P., Schuff, N., Liang, Z.P.: Denoising diffusion-weighted MR magnitude image sequences using low rank and edge constraints. In: 2012 9th IEEE International Symposium on Biomedical Imaging (ISBI), pp. 1401–1404. IEEE (2012)
124. Landman, B., Bazin, P.L., Prince, J., Hopkins, J.: Diffusion tensor estimation by maximizing Rician likelihood. In: Proceedings of IEEE 11th International Conference on Computer Vision, pp. 1–8 (2007)

125. Landman, B.A., Bazin, P.L., Prince, J.L.: Estimation and application of spatially variable noise fields in diffusion tensor imaging. Magn. Reson. Imaging **27**(6), 741–751 (2009)
126. Landman, B.A., Bazin, P.L., Smith, S.A., Prince, J.L.: Robust estimation of spatially variable noise fields. Magn. Reson. Med. **62**(2), 500–509 (2009)
127. Larkman, D.J., Nunes, R.G.: Parallel magnetic resonance imaging. Phys. Med. Biol. **52**, 15–55 (2007) (Invited Topical Review)
128. Lauterbur, P.: Image formation by induced local interactions: examples employing nuclear magnetic resonance. Nature **242**, 190–191 (1973)
129. Law, A., Kelton, W.D.: Simulation. Modeling and Analysis. Mc-Graw Hill, New York (1991)
130. Lee, J., Hoppel, K.: Noise modeling and estimation of remotely-sensed images. In: Geoscience and Remote Sensing Symposium, 1989. IGARSS'89. 12th Canadian Symposium on Remote Sensing., 1989 International, vol. 2, pp. 1005–1008 (1989)
131. Li, T., Wang, M., Li, T.: Estimating noise parameter based on the wavelet coefficients estimation of original image. In: 2010 International Conference on Challenges in Environmental Science and Computer Engineering (CESCE), vol. 1, pp. 126–129. IEEE (2010)
132. Liang, Z.P., Lauterbur, P.C.: Principles of Magnetic Resonance Imaging. A Signal Processing Perspective. IEEE Press, New York (2000)
133. Liévin, M., Luthon, F., Keeve, E.: Entropic estimation of noise for medical volume restoration. In: 2002. Proceedings. 16th International Conference on Pattern Recognition, vol. 3, pp. 871–874. IEEE (2002)
134. Lim, J.S.: Two Dimensional Signal and Image Processing. Prentice Hall, Englewood Cliffs (1990)
135. Liu, H., Yang, C., Pan, N., Song, E., Green, R.: Denoising 3D MR images by the enhanced non-local means filter for Rician noise. Magn. Reson. Imag. **28**(10), 1485–1496 (2010)
136. Liu, R.W., Shi, L., Huang, W., Xu, J., Yu, S.C.H., Wang, D.: Generalized total variation-based MRI Rician denoising model with spatially adaptive regularization parameters. Magn. Reson. Imaging **32**(6), 702–720 (2014)
137. Liu, W., Lin, W.: Additive white Gaussian noise level estimation in SND domain for images. IEEE Trans. Image Process. **22**(3), 872–883 (2013)
138. Liu, X., Huang, L., Guo, Z.: Adaptive fourth-order partial differential equation filter for image denoising. Appl. Math. Lett. **24**(8), 1282–1288 (2011)
139. Luisier, F., Wolfe, P.J.: Chi-square unbiased risk estimate for denoising magnitude MR images. In: 2011 18th IEEE International Conference on Image Processing (ICIP), pp. 1561–1564 (2011)
140. Lund, T.E., Madsen, K.H., Sidaros, K., Luo, W.L., Nichols, T.E.: Non-white noise in fMRI: does modelling have an impact? Neuroimage **29**(1), 54–66 (2006)
141. Lustig, M., Donoho, D., Pauly, J.M.: Sparse MRI: the application of compressed sensing for rapid MR imaging. Magn. Reson. Med. **58**(6), 1182–1195 (2007)
142. Lustig, M., Donoho, D., Santos, J., Pauly, J.: Compressed sensing MRI. IEEE Signal Process. Mag. **25**(2), 72–82 (2008)
143. Lysaker, M., Lundervold, A., Tai, X.: Noise removal using fourth order partial differential equations with applications to medical magnetic resonance imaging in space and time. IEEE Trans. Image Process. **12**(12) (2003)
144. Madore, B.: UNFOLD-SENSE: a parallel MRI method with self-calibration and artifact suppression. Magn. Reson. Med. **52**(2), 310–320 (2004)
145. Maggioni, M., Foi, A.: Nonlocal transform-domain denoising of volumetric data with groupwise adaptive variance estimation. In: IS&T/SPIE Electronic Imaging, pp. 82,960O–82,960O–8. International Society for Optics and Photonics (2012)
146. Maggioni, M., Katkovnik, V., Egiazarian, K., Foi, A.: Nonlocal transform-domain filter for volumetric data denoising and reconstruction. IEEE Trans. Image Process. **22**(1), 119–133 (2013)
147. Makitalo, M., Foi, A.: Optimal inversion of the Anscombe transformation in low-count Poisson image denoising. IEEE Trans. Image Process. **20**(1), 99–109 (2011)

148. Manjón, J., Carbonell-Caballero, J., Lull, J., García-Martí, G., Martı-Bonmatı, L., Robles, M.: MRI denoising using non-local means. Med. Image Anal. **12**, 514–523 (2008)
149. Manjón, J.V., Coupé, P., Buades, A.: MRI noise estimation and denoising using non-local PCA. Med. Image Anal. **22**, 35–47 (2015)
150. Manjón, J.V., Coupé, P., Buades, A., Collins, D.L., Robles, M.: New methods for MRI denoising based on sparseness and self-similarity. Med. Imag. Anal. **16**(1), 18–27 (2012)
151. Manjón, J.V., Coupé, P., Concha, L., Buades, A., Collins, D.L., Robles, M.: Diffusion weighted image denoising using overcomplete local PCA. PloS One **8**(9), e73021 (2013)
152. Manjón, J.V., Coupé, P., Marti-Bonmati, L., Collins, D.L., Robles, M.: Adaptive non-local means denoising of MR images with spatially varying noise levels. J. Magn. Reson. Imaging **31**(1), 192–203 (2010)
153. Mansfield, P., Grannel, P.: NMR diffraction in solids. J. Phys. Chem. **6**, 422–426 (1973)
154. Martín-Fernández, M., Muñoz-Moreno, E., Cammoun, L., Thiran, J.P., Westin, C.F., Alberola-López, C.: Sequential anisotropic multichannel Wiener filtering with Rician bias correction applied to 3D regularization of DWI data. Med. Image Anal. **13**(1), 19–35 (2009)
155. Martin-Fernandez, M., Villullas, S.: The EM method in a probabilistic wavelet-based MRI denoising. Comput. Math. Methods Med. **2015**, 182659-1–18265921 (2015)
156. Marzetta, T.: EM algorithm for estimating the parameters of multivariate complex Rician density for polarimetric SAR. Proc. ICASSP **5**, 3651–3654 (1995)
157. Maximov, I.I., Farrher, E., Grinberg, F.: Jon Shah, N.: Spatially variable Rician noise in magnetic resonance imaging. Med. Image Anal. **16**(2), 536–548 (2012)
158. McGibney, G., Smith, M.: Un unbiased signal-to-noise ratio measure for magnetic resonance images. Med. Phys. **20**(4), 1077–1078 (1993)
159. McGraw, T., Vemuri, B.C., Chen, Y., Rao, M., Mareci, T.: DT-MRI denoising and neuronal fiber tracking. Med. Image Anal. **8**, 95–111 (2004)
160. McVeigh, E., Henkelman, R., Bronskill, M.: Noise and filtration in magnetic resonance imaging. Med. Phys. **12**, 586–591 (1985)
161. Michailovich, O., Rathi, Y., Dolui, S.: Spatially regularized compressed sensing for high angular resolution diffusion imaging. IEEE Trans. Med. Imaging **30**(5), 1100–1115 (2011)
162. Miller, A.J., Joseph, P.M.: The use of power images to perform quantitative analysis on low snr MR images. Magn. Reson. Imaging **11**(7), 1051–1056 (1993)
163. Moon, N., Bullitt, E., Van Leemput, K., Gerig, G.: Automatic brain and tumor segmentation. In: Medical Image Computing and Computer-Assisted Intervention (MICCAI) 2002, pp. 372–379. Springer, Berlin (2002)
164. Muresan, D.D., Parks, T.W.: Adaptive principal components and image denoising. IEEE Int. Conf. Image Process. **1**, 101–104 (2003)
165. Noh, J., Solo, V.: Rician distributed functional MRI: asymptotic power analysis of likelihood ratio tests for activation detection. In: 2010 IEEE International Conference on Acoustics Speech and Signal Processing (ICASSP), pp. 477–480 (2010)
166. Noh, J., Solo, V.: Rician distributed fMRI: asymptotic power analysis and Cramer-Rao lower bounds. IEEE Trans. Signal Proccess. **59**(3), 1322–1328 (2011)
167. Nowak, R.: Wavelet-based Rician noise removal for magnetic resonance imaging. IEEE Trans. Image Process. **8**(10), 1408–1419 (1999)
168. Olsen, S.I.: Estimation of noise in images: an evaluation. CVGIP. Gr. Model. Image Process. **55**(4), 319–323 (1993)
169. Oppeinhein, A., Schafer, R., Stockham, T.: Nonlinear filtering of multiplied and convolved signals. Proc. IEEE USA **56**(8), 1–264 (1968)
170. Otsu, N.: A threshold selection method from gray-scale histogram. IEEE Trans. Syst. Man Cybern. **9**(1), 62–66 (1979)
171. Özarslan, E., Shepherd, T.M., Vemuri, B.C., Blackband, S.J., Mareci, T.H.: Resolution of complex tissue microarchitecture using the diffusion orientation transform (DOT). Neuroimage **31**(3), 1086–1103 (2006)
172. Pajevic, S., Basser, P.J.: Parametric and non-parametric statistical analysis of DT-MRI data. J. Magn. Reson. **161**(1), 1–14 (2003)

173. Pan, X., Zhang, X., Lyu, S.: Blind local noise estimation for medical images reconstructed from rapid acquisition. In: SPIE Medical Imaging, pp. 83,143R–83,143R (2012)
174. Papoulis, A.: Probability. Random Variables and Stochastic Processes. Mc-Graw Hill, New York (1991)
175. Park, S., Park, J.: Adaptive self-calibrating iterative GRAPPA reconstruction. Magn. Reson. Med. **67**(6), 1721–1729 (2012)
176. Parker, G.J., Schnabel, J.A., Symms, M.R., Werring, D.J., Barker, G.J.: Nonlinear smoothing for reduction of systematic and random errors in diffusion tensor imaging. J. Magn. Reson. Imaging **11**(6), 702–710 (2000)
177. Perona, P., Malik, J.: Scale-space and edge detection using anisotropic diffusion. IEEE Trans. Pattern Anal. Mach. Intell. **12**(7), 629–639 (1990)
178. Pieciak, T.: The maximum spacing noise estimation in single-coil background MRI data. In: IEEE International Conference on Image Processing (ICIP), pp. 1743–1747 (2014)
179. Pieciak, T., Vegas-Sánchez-Ferrero, G., Aja-Fernández, S.: Non-stationary Rician noise estimation in parallel MRI using a single image:a variance-stabilizing approach. IEEE Trans. Pattern Anal. Mach. Intell. (2016). Submitted
180. Pieciak, T., Vegas-Sánchez-Ferrero, G., Aja-Fernández, S.: Variance stabilization of noncentral-chi data: application to noise estimation in MRI. In: 2016 IEEE International Symposium on Biomedical Imaging: From Nano to Macro (2016)
181. Pižurica, A., Philips, W., Lemahieu, I., Acheroy, M.: A versatile Wavelet domain noise filtration technique for medical imaging. IEEE Trans. Med. Imaging **22**(3), 323–331 (2003)
182. Pizurica, A., Wink, A.M., Vansteenkiste, E., Philips, W., Roerdink, B.J.: A review of wavelet denoising in MRI and ultrasound brain imaging. Current Med. Imaging Rev. **2**(2), 247–260 (2006)
183. Polzehl, J., Spokoiny, V.: Propagation-separation approach for local likelihood estimation. Probab. Theory Relat. Fields **135**(3), 335–362 (2006)
184. Poot, D., Klein, S.: Detecting statistically significant differences in quantitative MRI experiments, applied to diffusion tensor imaging. IEEE Trans. Med. Imaging **34**(5), 1164–1176 (2015)
185. Poupon, C., Roche, A., Dubois, J., Mangin, J.F., Poupon, F.: Real-time MR diffusion tensor and Q-Ball imaging using Kalman filtering. Med. Image Anal. **12**(5), 527–534 (2008)
186. Pruessmann, K.P., Weiger, M., Scheidegger, M.B., Boesiger, P.: SENSE: sensitivity encoding for fast MRI. Magn. Reson. Med. **42**(5), 952–62 (1999)
187. Purcell, E., Torrey, H., Pound, R.: Resonance absorption by nuclear magnetic moments in a solid. Phys. Rev. **69**, 37 (1946)
188. Rajan, J., Poot, D., Juntu, J., Sijbers, J.: Noise measurement from magnitude MRI using local estimates of variance and skewness. Phys. Med. Biol. **55**(16), N441 (2010)
189. Rajan, J., Poot, D., Juntu, J., Sijbers, J.: Maximum likelihood estimation-based denoising of magnetic resonance images using restricted local neighborhoods. Phys. Med. Biol. **56**(16), 5221–5234 (2011)
190. Rajan, J., Veraart, J., Audekerke, J.V., Verhoye, M., Sijbers, J.: Nonlocal maximum likelihood estimation method for denoising multiple-coil magnetic resonance images. Magn. Reson. Imaging **20** (2012)
191. Rangachari, S., Loizou, P.C.: A noise-estimation algorithm for highly non-stationary environments. Speech Commun. **48**(2), 220–231 (2006)
192. Rank, K., Lendl, M., Unbehauen, R.: Estimation of image noise variance. IEE Proc.-Vis. Image. Signal Process. **146**(2), 80–84 (1999)
193. Restom, K., Behzadi, Y., Liu, T.T.: Physiological noise reduction for arterial spin labeling functional MRI. NeuroImage **31**(3), 1104–1115 (2006)
194. Robson, P., Grant, A., Madhuranthakam, A., Lattanzi, R., Sodickson, D., McKenzie, C.: Comprehensive quantification of signal-to-noise ratio and g-factor for image-based and k-space-based parallel imaging reconstructions. Magn. Reson. Med. **60**, 895 (2008)
195. Roemer, P., Edelstein, W., Hayes, C., Souza, S., Mueller, O.: The NMR phased array. Magn. Reson. Med. **16**, 192–225 (1990)

196. Rousseeuw, P.J., Croux, C.: Alternatives to the median absolute deviation. J. Am. Stat. Assoc. **88**(424), 1273–1283 (1993)
197. Roy, S., Carass, A., Bazin, P.L., Resnick, S., Prince, J.L.: Consistent segmentation using a Rician classifier. Med. Image Anal. **16**(2), 524–535 (2012)
198. Rudin, L.I., Osher, S., Fatemi, E.: Nonlinear total variation based noise removal algorithms. Phys. D: Nonlinear Phenom. **60**(1), 259–268 (1992)
199. Salmeri, M., Mencattini, A., Ricci, E., Salsano, A.: Noise estimation in digital images using fuzzy processing. In: Proceedings of the IEEE International Conference on Image Processing, vol. 1, pp. 517–520. Thessaloniki (Greece) (2001)
200. Salvador, R., Peña, A., Menon, D.K., Carpenter, T., Pickard, J., Bullmore, E.T.: Formal characterization and extension of the linearized diffusion tensor model. Hum. Brain Mapp. **24**, 144–155 (2005)
201. Samsonov, A.A., Johnson, C.R.: Noise-adaptive nonlinear diffusion filtering of MR images with spatially varying noise levels. Magn. Reson. Med. **52**(4), 798–806 (2004)
202. Sapiro, G., Ringach, D.L.: Anisotropic diffusion of multivalued images with applications to color filtering. IEEE Trans. Image Process. **5**, 1582–1586 (1996)
203. Schmid, V.J., Whitcher, B., Padhani, A.R., Taylor, N.J., Yang, G.Z.: A Bayesian hierarchical model for the analysis of a longitudinal dynamic contrast-enhanced MRI oncology study. Magn. Reson. Med. **61**(1), 163–174 (2009)
204. Shafiee, M.J., Haider, S.A., Wong, A., Lui, D., Cameron, A., Modhafar, A., Fieguth, P., Haider, M.A.: Apparent ultra-high-value diffusion-weighted image reconstruction via hidden conditional random fields. IEEE Trans. Med. Imaging **34**(5), 1111–1124 (2015)
205. Shin, D.H., Park, R.H., Yang, S., Jung, J.H.: Block-based noise estimation using adaptive Gaussian filtering. IEEE Trans. Consumer Electron. **51**(1), 218–226 (2005)
206. Shin, D.H., Park, R.H., Yang, S., Jung, J.H.: Noise estimation using adaptive Gaussian filtering. IEEE Trans. Consumer Electron. **51**(1), 218–226 (2005)
207. Sijbers, J., den Dekker, A.J., Van der Linden, A., Verhoye, M., Van Dyck, D.: Adaptive anisotropic noise filtering for magnitude MR data. Magn. Reson. Imaging **17**(10), 1533–1539 (1999)
208. Sijbers, J., den Dekker, A., Scheunders, P., Van Dyck, D.: Maximum-likelihood estimation of Rician distribution parameters. IEEE Trans. Med. Imaging **17**(3), 357–361 (1998)
209. Sijbers, J., den Dekker, A., Van Audekerke, J., Verhoye, M., Van Dyck, D.: Estimation of the noise in magnitude MR images. Magn. Reson. Imaging **16**(1), 87–90 (1998)
210. Sijbers, J., den Dekker, A.J.: Maximum likelihood estimation of signal amplitude and noise variance form MR data. Magn. Reson. Imaging **51**, 586–594 (2004)
211. Sijbers, J., den Dekker, A.J., Poot, D., Verhoye, M., Van Camp, N., Van der Linden, A.: Robust estimation of the noise variance from background MR data. In: Proceedings of SPIE. Medical Imaging 2006: Image Processing, vol. 6144, pp. 2018–2028 (2006)
212. Sijbers, J., den Dekker, A.J., Van Dyck, D., Raman, E.: Estimation of signal and noise from Rician distributed data. In: Proceedings of the International Conference on Signal Processing and Communication, pp. 140–142. Las Palmas de Gran Canaria (1998)
213. Sijbers, J., Poot, D., den Dekker, A.J., Pintjens, W.: Automatic estimation of the noise variance from the histogram of a magnetic resonance image. Phys. Med. Biol. **52**, 1335–1348 (2007)
214. Simon, M.K.: Probability Distributions Involving Gaussian Random Variables. Kluwer Academic Publishers, Boston (2002)
215. Simoncelli, E., Adelson, E.: Noise removal via bayesian wavelet coring. In: Proceedings of International Conference on Image Processing, 1996, vol. 1, pp. 379–382 (1996)
216. Siyal, M.Y., Yu, L.: An intelligent modified fuzzy c-means based algorithm for bias estimation and segmentation of brain MRI. Pattern Recognit. Lett. **26**(13), 2052–2062 (2005)
217. Sodickson, D., Manning, W.: Simultaneous acquisition of spatial harmonics (SMASH): fast imaging with radiofrequency coil arrays. Magn. Reson. Med. **38**, 591–603 (1997)
218. Soltanian-Zadeh, H., Windham, J.P., Peck, D.J., Yagle, A.E.: A comparative analysis of several transformations for enhancement and segmentation of magnetic resonance image scene sequences. IEEE Trans. Med. Imaging **11**(3), 302–318 (1992)

219. Starck, J.L., Murtagh, F.: Automatic noise estimation from the multiresolution support. Publ. Astron. Soc. Pac. **110**, 193–199 (1998)
220. Stehling, M., Turner, R., Mansfield, P.: Echo-planar imaging: magnetic resonance imaging in a fraction of a second. Science **254**(5028), 43–50 (1991)
221. Stejskal, E.O., Tanner, J.E.: Spin diffusion measurements: spin echoes in the presence of a time-dependent field gradient. J. Chem. Phys. **42**, 288–292 (1965)
222. Tabelow, K., Voss, H.U., Polzehl, J.: Local estimation of the noise level in MRI using structural adaptation. Med. Image Anal. **20**(1), 76–86 (2015)
223. Tai, S.C., Yang, S.M.: A fast method for image noise estimation using laplacian operator and adaptive edge detection. In: ISCCSP 2008. 3rd International Symposium on Communications, Control and Signal Processing, 2008, pp. 1077–1081. IEEE (2008)
224. Tan, H., Maldjian, J., Pollock, J., Burdette, J., Yang, L., Deibler, A., Kraft, R.: A fast, effective filtering method for improving clinical pulsed arterial spin labeling MRI. J. Magn. Reson. Imaging **29**(5), 1134–1139 (2009)
225. Thomas, C.G., Harshman, R.A., Menon, R.S.: Noise reduction in BOLD-based fMRI using component analysis. Neuroimage **17**(3), 1521–1537 (2002)
226. Thünberg, P., Zetterberg, P.: Noise distribution in SENSE- and GRAPPA- reconstructed images: a computer simulation study. Magn. Reson. Imaging **25**, 1089–94 (2007)
227. Tristán-Vega, A., Aja-Fernández, S.: Joint LMMSE estimation of DWI data for DTI processing. In: Proceedings of MICCAI 08. Lecture Notes on Computer Science, vol. 5242, pp. 27–34 (2008)
228. Tristán-Vega, A., Aja-Fernández, S.: DWI filtering using joint information for DTI and HARDI. Med. Image Anal. **14**(2), 205–218 (2010)
229. Tristán-Vega, A., Aja-Fernández, S., Westin, C.F.: Least squares for diffusion tensor estimation revisited: propagation of uncertainty with Rician and non-Rician signals. NeuroImage **59**, 4032–4043 (2012)
230. Tristan-Vega, A., Brion, V., Vegas-Sanchez-Ferrero, G., Aja-Fernandez, S.: Merging squared-magnitude approaches to DWI denoising: an adaptive wiener filter tuned to the anatomical contents of the image. In: 2013 35th Annual International Conference of the IEEE Engineering in Medicine and Biology Society (EMBC), pp. 507–510. IEEE (2013)
231. Tristán-Vega, A., García-Pérez, V., Aja-Fernández, S., Westin, C.F.: Efficient and robust non-local means denoising of MR data based on salient features matching. Comput. Methods Programs Biomed. **105**, 131–144 (2012)
232. Tristán-Vega, A., Westin, C.F., Aja-Fernández, S.: Bias of least squares approaches for diffusion tensor estimation from array coils in DT–MRI. In: MICCAI 2009. Lecture Notes in Computer Science, vol. 5761, pp. 919–926 (2009)
233. Tristán-Vega, A., Westin, C.F., Aja-Fernández, S.: Estimation of fiber orientation probability density functions in high angular resolution diffusion imaging. NeuroImage **47**(2), 638–650 (2009)
234. Tristán-Vega, A., Westin, C.F., Aja-Fernández, S.: A new methodology for the estimation of fiber populations in the white matter of the brain with the Funk-Radon transform. NeuroImage **49**(2), 1301–1315 (2010)
235. Tuch, D.S.: Q-ball imaging. Magn. Reson. Med. **52**(6), 1358–1372 (2004)
236. Uecker, M., Hohage, T., Block, K.T., Frahm, J.: Image reconstruction by regularized nonlinear inversionjoint estimation of coil sensitivities and image content. Magn. Reson. Med. **60**(3), 674–682 (2008)
237. Vegas-Sanchez-Ferrero, G., Ramos-Llorden, G., de Luis-Garcia, R., Tristan-Vega, A., Aja-Fernandez, S.: Anisotropic diffusion filtering for correlated multiple-coil MRI. In: 2013 35th Annual International Conference of the IEEE Engineering in Medicine and Biology Society (EMBC), pp. 2956–2959 (2013)
238. Vegas-Sánchez-Ferrero, G., Tristán-Vega, A., Aja-Fernández, S., Martín-Fernández, M., Palencia, C., Deriche, R.: Anisotropic LMMSE denoising of MRI based on statistical tissue models. In: 2012 9th IEEE International Symposium on Biomedical Imaging (ISBI), pp. 1519–1522. IEEE (2012)

239. Veraart, J., Rajan, J., Peeters, R.R., Leemans, A., Sunaert, S., Sijbers, J.: Comprehensive framework for accurate diffusion MRI parameter estimation. Magn. Reson. Med. **70**(4), 972–984 (2013)
240. Wang, J., Kluge, T., Nittka, M., Jellus, V., Kuehn, B., Kiefer, B.: Parallel acquisition techniques with modified SENSE reconstruction mSENSE. In: Proceedings of the First Würzburg Workshop on Parallel Imaging Basics and Clinical Applications, p. 89 (2001)
241. Weaver, J., Xu, Y., Healy, D., Driscoll, J.: Filtering MR images in the wavelet transform domain. Magn. Reson. Med. **21**(3), 288–295 (1991)
242. Weickert, J.: Anisotropic Diffusion in Image Processing. Teubner-Verlag, Stuttgart (1998)
243. Weiger, M., Pruessmann, K.P., Boesiger, P.: 2D SENSE for faster 3D MRI. Magn. Reson. Mater. Phys. Biol. Med. **14**(1), 10–19 (2002)
244. Weisskoff, R., Baker, J., Belliveau, J., Davis, T., Kwong, K., Cohen, M., Rosen, B.: Power spectrum analysis of functionally-weighted MR data: whats in the noise. In: Proceedings of the International Society of Magnetic Resonance in Medicine, vol. 1 (1993)
245. Wells III, W.M., Grimson, W.E.L., Kikinis, R., Jolesz, F.A.: Adaptive segmentation of MRI data. IEEE Trans. Med. Imaging **15**(4), 429–442 (1996)
246. Welvaert, M., Durnez, J., Moerkerke, B., Verdoolaege, G., Rosseel, Y.: neuRosim: an R package for generating fMRI data. J. Stat. Softw. **44**(10) (2011)
247. Wiest-Daesslé, N., Prima, S., Coupé, P., Morrissey, S., Barillot, C.: Rician noise removal by non-local means filtering for low signal-to-noise ratio MRI: applications to DT-MRI. Medical Image Computing and Computer-Assisted Intervention. Lecture Notes in Computer Science, vol. 5242, pp. 171–179. Springer, Berlin (2008)
248. Wirestam, R., Bibic, A., Lätt, J., Brockstedt, S., Ståhlberg, F.: Denoising of complex MRI data by wavelet-domain filtering: application to high-b-value diffusion-weighted imaging. Magn. Reson. Med. **56**(5), 1114–1120 (2006)
249. Wood, J.C., Johnson, K.M.: Wavelet packet denoising of magnetic resonance images: importance of Rician noise at low SNR. Magn. Reson. Med. **41**(3), 631–635 (1999)
250. Wu, X., Bricq, S., Collet, C.: Brain MRI segmentation and lesion detection using generalized Gaussian and Rician modeling. In: Dawant, B.M., Haynor, D.R. (eds.) Medical Imaging 2011: Image Processing, vol. 7962. SPIE (2011)
251. Yang, G.Z., Burger, P., Firmin, D.N., Underwood, S.R.: Structure adaptive anisotropic filtering for magnetic resonance images. Lect. Notes Comput. Sci. **970**, 384–391 (1995)
252. Yang, J., Fan, J., Ai, D., Zhou, S., Tang, S., Wang, Y.: Brain MR image denoising for Rician noise using pre-smooth non-local means filter. Biomed. Eng. OnLine **14**(2), 1–20 (2015)
253. Yaroslavsky, L.P., Egiazarian, K.O., Astola, J.T.: Transform domain image restoration methods: review, comparison, and interpretation. In: SPIE Proceedings, Nonlinear Image Processing and Pattern Analysis XII (2001)
254. Yeh, E.N.: Advanced image reconstruction in parallel mahnetic resonance imaging: constraints and solutions. Ph.D. thesis, MIT (2005)
255. Ying, L., Sheng, J.: Joint image reconstruction and sensitivity estimation in sense (jsense). Magn. Reson. Med. **57**(6), 1196–1202 (2007)
256. Yu, J., Agarwal, H., Stuber, M., Schär, M.: Practical signal-to-noise ratio quantification for sensitivity encoding: application to coronary MR angiography. J. Magn. Reson. **33**(6), 1330–1340 (2011)
257. Zhang, B., Fadili, J.M., Starck, J.L.: Wavelets, Ridgelets, and curvelets for poisson noise removal. IEEE Trans. Image Process. **17**(7), 1093–1108 (2008)
258. Zhang, X., Xu, Z., Jia, N., Yang, W., Feng, Q., Chen, W., Feng, Y.: Denoising of 3D magnetic resonance images by using higher-order singular value decomposition. Med. Image Anal. **19**(1), 75–86 (2015)

Index

S. Aja-Fernández and G. Vegas-Sánchez-Ferrero,
Statistical Analysis of Noise in MRI, DOI 10.1007/978-3-319-39934-8